Laser Light Scattering Evidence for a Common Wormlike Growth Structure of Mixed Micelles in Bile Salt− and Straight-Chain Detergent−Phosphatidylcholine Aqueous Systems: Relevance to the Micellar Structure of Bile†

David E. Cohen,‡,§ George M. Thurston,||,⊥ Richard A. Chamberlin,||,▽ George B. Benedek,|| and Martin C. Carey*,‡

Department of Medicine, Harvard Medical School, Brigham and Women's Hospital and Harvard Digestive Diseases Center, Boston, Massachusetts 02115, and Department of Physics and Center for Materials Science and Engineering, Massachusetts Institute of Technology, Cambridge, Massachusetts 02139

Received January 24, 1998; Revised Manuscript Received June 4, 1998

ABSTRACT: We employed quasielastic and static light scattering to measure apparent values of the mean hydrodynamic radii $(R_h)_{app}$, molecular weights (M_{app}), and radii of gyration $(R_g)_{app}$ in solutions containing mixed micelles composed of bile salts (cholate and taurochenodeoxycholate, both cholanoyl derivatives) and the glycoacyl chain detergent, octyl glucoside, with egg yolk phosphatidylcholine (EYPC) as functions of total lipid concentration (0.1−10 g/dL), EYPC/detergent molar ratio (0−1.2), and ionic strength (0.15−0.4 M NaCl) at 20 °C and 1 atm. As the mixed micellar phase boundaries were approached by dilution, $(R_h)_{app}$, M_{app}, and $(R_g)_{app}$ values increased markedly by up to 20-fold. For each micellar system, the scaling ratios $(R_h)_{app}/M_{app}^{1/2}$ and $(R_g)_{app}/(R_h)_{app}$ remained essentially constant at 0.018 nm/(g/mol)$^{1/2}$ and 1.5 (dimensionless), respectively, despite large variations in total lipid concentration, detergent molecular species, and ionic strength. Refined data analysis is inconsistent with a flat "mixed-disc" model for bile salt−EYPC micelles [Mazer, N. A., Benedek, G. B., and Carey, M. C. (1980) *Biochemistry 19*, 601] and octyl glucoside−EYPC micelles principally because the numerical value of $(R_h)_{app}/M_{app}^{1/2}$ corresponds to a hypothetical disk thickness of ∼1 nm, which is 4-fold smaller than the bimolecular width of EYPC molecules, and for a disk, $(R_g)_{app}/(R_h)_{app}$ ratios should be close to 1 at low total lipid concentrations. Assuming disc-shaped micelles, we show that intermicellar excluded volume interactions would have only a minor effect on M_{app} and cannot account for the unrealistic disk thickness. Instead, locally cylindrical, semiflexible wormlike micelles of diameter $d = 4$ nm and persistence length $\xi_p = 17$ nm in solution are compatible with the observed $(R_h)_{app}/M_{app}^{1/2}$ and $(R_g)_{app}/(R_h)_{app}$ values when intermicellar excluded-volume interactions are considered. With EYPC/taurochenodeoxycholate = 0.6 and EYPC/cholate = 1.0 in 0.15 M NaCl, independent micelles grow upon dilution and use of the second virial coefficient [Egelhaaf, S. U., and Schurtenberger, P. (1994) *J. Phys. Chem. 98*, 8560] is adequate for estimating micellar weights. The systems EYPC/cholate = 1.0 in 0.4 M NaCl, EYPC/cholate = 1.2 in 0.15 M NaCl, and EYPC/octyl glucoside = 0.13 in 0.15 M NaCl all form highly overlapping, semidilute polymer solutions, which mimic the observed scaling ratios. In such semidilute systems, use of the second virial coefficient alone to account for intermicellar interactions is inadequate for estimating micellar weights. The results of the present study, in combination with locations of known phase boundaries of the ternary bile salt−EYPC−water phase diagram at high dilution, suggest that elongation, as well as entanglement of wormlike mixed micelles may occur at concentrations approaching the micellar phase limit.

Aqueous mixed micellar solutions of steroidal or straight-chain detergents with long-chain phosphatidylcholine (PC)[1] are of considerable scientific and biomedical interest. Detergent−PC micelles ensure the thermodynamic stability of vertebrate and invertebrate biles during solubilization and transport of cholesterol (*1*, *2*) and have been employed to reconstitute phospholipid vesicles for studies of membrane proteins (*3*, *4*). Aqueous monomeric solubilities of biological

† Supported in part by Grants DK36588, AM34854, and GM07258 from the National Institutes of Health (M.C.C.), NIH Grant DK48873 and postdoctoral fellowships from the Medical Foundation (Boston) and the American Liver Foundation (D.E.C.), National Science Foundation Grant DMR 7680895-A02 to the Center for Materials Science and Engineering, MIT, and National Science Foundation Grant 7707666-CHE (R.A.C., G.M.T., and G.B.B.).

* Correspondence should be addressed to this author at Department of Medicine, Gastroenterology Division, Brigham and Women's Hospital, 75 Francis St., Boston, MA 02115. Phone (617) 732-5822; Fax (617) 730-5807; email mccarey@bics.bwh.harvard.edu.

‡ Harvard.

§ Present addresses: Marion Bessin Liver Research Center, Albert Einstein College of Medicine, Bronx, NY 10461.

|| MIT.

⊥ Present address: Center for Ophthalmic Research, Brigham and Women's Hospital, Boston, MA 02115.

▽ Present address: Caltech Sub-mm Observatory, 111 Nowelo Street, Hilo, HI 96720.

[1] Abbreviations: QLS, quasielastic light scattering; HPLC, high-performance liquid chromatography; cholate, 3α,7α,12α-trihydroxy-5β-cholanoate; taurochenodeoxycholate, taurine conjugate of 3α,7α-dihydroxy-5β-cholanoate (both as Na^+ salts); EYPC, egg yolk phosphatidylcholine (lecithin); PC, phosphatidylcholine; OG, octyl glucoside (octyl β-D-glucopyranoside).

10.1021/bi980182y CCC: $15.00
Published on Web 10/01/1998

PC molecules are extremely low, approximating 10^{-10} M (*5*). However, in the presence of physiological concentrations of common bile salts (BS), which are the alkali salts of hydroxyl-substituted cholanoic acids, or straight-chain analogues of crustacean bile salts such as octyl glucoside (OG), a nonionic detergent, substantial concentrations (up to ~100 mM in the case of bile salts) of long-chain PC may be solubilized as mixed micelles (*1*−*3, 6*). The macroscopic interactions between these very dissimilar soluble amphiphiles (BS and OG) and insoluble swelling (PC) amphiphiles are governed by total and relative concentrations of the lipids in water at fixed temperature and pressure, and are embodied in detergent−PC−water phase diagrams (*1*−*3, 6*). Because monomeric solubilities of these detergents and long-chain PC differ by at least 6 orders of magnitude, dilution of mixed micellar solutions within their respective micellar zones increases the relative PC content and decreases the relative detergent content of the micellar particles, resulting in an altered lipid ratio that leads to mixed micellar growth (*1, 6, 7*). This occurs because detergent molecules migrate from mixed micelles to the water component to replenish the intermicellar detergent concentration, a process that was first followed noninvasively by quasielastic light scattering spectroscopy (QLS) (*7*).

On the basis of earlier QLS studies, Mazer et al. (*7*) proposed a mixed disk model for the bile salt−long-chain PC micelles of bile. This model was a minor modification of the simple disk model proposed by Small (*8*) and Dervichian (*9*) for bile salt−EYPC mixed micelles. These authors postulated the disk structure on the basis of X-ray diffraction analysis of bile salt-EYPC liquid crystalline phases (*8*) as well as from examination of the hydrophilic−hydrophobic balance of the molecules (*9*). Mazer et al. (*7*) found that the mixed disk model predicted the mixed micellar growth observed in model bile systems by QLS when this was achieved either by dilution or by varying the EYPC/bile salt ratio at constant concentration. However, more recent studies employing small-angle neutron scattering (*10, 11*), high-performance liquid chromatography (*12*), cryo-transmission electron microscopy (*13*), and light scattering (*14*) have questioned growth of bile salt−PC mixed micelles via the mixed disk model and have shown that they may form locally cylindrical rodlike particles. In addition, octyl glucoside−PC mixed micelles appear to grow with similar morphology (*3*) despite the strikingly different molecular structures of octyl glucoside and common bile salts (*15*).

To elucidate the sizes, shapes, and possible molecular structure(s) of bile salt− and octyl glucoside−EYPC mixed micelles, we reinvestigated these systems employing both QLS and static light scattering techniques (*16*−*19*).[2] Apparent molecular weights[3] (M_{app}), radii of gyration $(R_g)_{app}$, and mean hydrodynamic radii $(R_h)_{app}$ of mixed micelles were determined as functions of total lipid concentration. These data extend our earlier determinations of mixed micellar R_h sizes and relative scattered light intensity values of analogous bile salt−EYPC systems (*7*). Moreover, the present data analysis incorporates the effect of intermicellar interactions on M_{app} to the level of the second virial coefficient and allows us to exclude a dilute solution of mixed-disk structures. We demonstrate that the data are instead consistent with a "locally cylindrical" model of mixed micelles which grow as flexible, wormlike objects. The earlier R_h values of Mazer et al. (*7*) are shown to be entirely consistent with this alternative model. The wormlike structure provides a basis for understanding phase transitions from mixed micelles to a hexagonal (H_I) liquid crystalline phase that occur upon dilution of EYPC−bile salt mixed micellar solutions, which is then followed by a separation of unilamellar vesicles (*1, 6*). This series of phase transitions is of fundamental relevance to the structure of bile, since it is essentially reversed during bile formation (*20, 21*).

EXPERIMENTAL PROCEDURES

Materials. Sodium salts of cholate (3α,7α,12α-trihydroxy-5β-cholanoate), and taurochenodeoxycholate, the taurine conjugate of 3α,7α-dihydroxy-5β-cholanoate (Calbiochem, San Diego, CA) were purified to 98% and each gave a single spot on thin-layer chromatography following a 200 μg sample application. Highest (Ultrol) grade octyl glucoside (octyl β-D-glucopyranoside) was obtained from Calbiochem and used without further purification. Grade I EYPC (Lipid Products, South Nutfield, Surrey, U.K.) was >99% pure (*22*) by high-performance liquid chromatography (HPLC) and thin-layer chromatography (200 μg sample application). All other chemicals and solvents were ACS- or reagent-grade purity (Fisher Scientific, Medford, MA). NaCl was roasted at 600 °C for 4 h to oxidize and remove organic impurities. Pyrex-brand glassware was alkali-washed for 24 h (EtOH-2M KOH, 1:1, v:v) followed by 24 h acid washing (1M HNO_3) and rinsed thoroughly with purified water. Water was filtered, ion exchanged, glass distilled (Corning Glass Works, Corning, NY) and further purified using a MilliQ water system (Millipore, Bedford, MA).

Mixed Micellar Solutions. Following coprecipitation from stock solutions in $CHCl_3$/MeOH (1:1, v:v), dried detergent−EYPC films were dissolved in aqueous solution (0.15−0.40 M NaCl, pH ~7, or in the case of cholate, 0.01 M $NaHCO_3$/Na_2CO_3 plus 0.14 M NaCl at pH 9.0) that included 3.0 mM NaN_3 as an antimicrobial agent (*23*) to achieve the desired total lipid concentration. In all bile salt systems, the pH values ensured complete bile salt ionization (*24*). Prior to light scattering experiments, mixed micellar solutions were equilibrated for 24 h at 20 °C under an atmosphere of argon and then centrifuged in a model L preparative ultracentrifuge (Beckman, Fullerton, CA) for 1−3 h at 10000*g* to sediment dust.

Laser Light Scattering Spectroscopy. Quasielastic and static light scattering spectroscopy utilize temporal and spatial variations in intensity of scattered laser light for physical−chemical analysis of particles in solution. By appropriate analysis one can determine sizes, polydispersities, molecular weights, and shapes of macromolecules with considerable precision. Because comprehensive reviews of laser light

[2] Portions of this work were presented at the Materials Research Society Fall Meeting, Boston, MA, 1989, at the Third International Symposium on Complex Fluids in Santa Barbara, CA, 1989, and at Falk Symposium 58−Bile Acids as Therapeutic Agents, Freiburg, Germany, 1990, and published in abstract form (*16, 17, 20*).

[3] Apparent molecular weight (M_{app}) is the molecular weight (M) derived from the light scattering intensity measurements assuming no interactions between micelles, as would be the case at high dilution. At semidilute (i.e., higher) lipid concentrations, intermicellar interactions affect the light scattering intensity and therefore M_{app} deviates from the true M.

scattering theory and applications are available (*25*−*27*), we summarize herein only experimental and theoretical details pertinent to the present investigation.

Instrumentation. We employed a laser light scattering spectrophotometer based on a design by Haller et al. (*19*), the details of which are presented elsewhere (*18*). Briefly, a vertically polarized argon-ion laser (Coherent Innova, model 90-5) operating at a wavelength (λ) of 488 nm was employed as a light source. Lipid samples were housed in a circulating dust-free water bath designed for refractive index matching (*18*) with a temperature maintained at 20 ± 0.1 °C employing a Neslab model RTE-8 apparatus (Portsmouth, NH). In the present configuration, scattered laser light was detected at 12 separate scattering angles ranging from 11.5° to 162.6°. Since repositioning a photomultiplier tube introduces the possibility of optical misalignments, we avoided such experimental errors by positioning individual lenses and computer-controlled shutter systems at each scattering angle. Light from each lens was transmitted via individual optical fibers to a remote photomultiplier tube, which was in turn interfaced with a 128-channel autocorrelator (Langley-Ford, model 1096, Amherst, MA). Control of the apparatus and data acquisition and analysis were performed on-line employing a Digital MicroVax II computer (Digital Equipment, Maynard, MA).

Data Analysis: *Quasielastic Light Scattering.* Particle diffusion coefficients D were measured at each scattering angle by analyzing intensity autocorrelation functions according to the method of cumulants (*28*). The mean diffusion coefficient of the micellar solution was calculated from a plot of mean diffusion coefficient versus scattering angle (*18*). $(R_h)_{app}$ values were calculated according to the Stokes−Einstein relationship utilizing the viscosity of the solvent.

Static Light Scattering. Static light scattering employed the same configuration of the light scattering apparatus as above to measure mean apparent molecular weight (M_{app}) and radius of gyration $(R_g)_{app}$ of the mixed micelles. From mean scattered light intensity $I(\theta)$ measured at each scattering angle θ, Rayleigh ratios [$R(\theta)$] were determined by normalizing $I(\theta)$ values to light scattered by benzene and toluene standards (*18*). The individual $(R_g)_{app}$ and M_{app} values of the mixed micelles were calculated according to the formula (*29*)

$$R(\theta)^{-1} = [1 + {}^1/_3(R_g)_{app}{}^2 q(\theta)^2]/(M_{app}KC) \qquad (1)$$

where $q(\theta) = (4\pi n/\lambda) \sin(\theta/2)$ represents the magnitude (nanometers^{-1}) of the scattering vector, n is the refractive index of the solution, C is the micellar lipid concentration (equal to the total lipid concentration minus the intermicellar concentration of the monomer in mass/volume),[4] and $K = 4\pi^2 n^2 (dn/dC)^2/\lambda^4 N_a$, where N_a is Avogadro's number. Values of $R(\theta)^{-1}$ varied linearly as functions of $q(\theta)^2$. By linear least-squares analysis, M_{app} was determined from the intercept $R(0)^{-1}$, and $(R_g)_{app}$ values were calculated from the slope of the line. To determine dn/dC, refractive index (n) values were measured with an Abbé-type refractometer (Bausch and Lomb, model Abbé-3L). The lipid samples of known concentrations were prepared by serial dilutions of concentrated micellar solutions (10 g/dL) with buffer (see Experimental Design). Because n values varied linearly as functions of C (data not shown), dn/dC was calculated from the slope of each line fitted by linear least-squares analysis.

Experimental Design. Concentrated (5 or 10 g/dL) mixed micellar solutions were prepared from EYPC and either cholate (EYPC/cholate molar ratios = 0−1.2), taurochenodeoxycholate (EYPC/taurochenodeoxycholate molar ratio = 0.6), or octyl glucoside (EYPC/octyl glucoside molar ratio = 0.13). Following collection of each data set, the micellar solutions were diluted with buffer at constant pH to a desired total lipid concentration and then another laser light scattering data set was collected and analyzed. To confirm the internal consistency of dilution, a series of total lipid concentrations for each detergent−EYPC mixture, were prepared by direct dilution from stock solutions to the desired concentration. All original and diluent compositions were designed to fall within micellar zones of their respective detergent−EYPC−water phase diagrams (*30*, *32*). Precise dilution within the micellar phases was confirmed experimentally when serial or direct dilution to a desired total lipid concentration yielded identical $(R_h)_{app}$ values that did not display any appreciable time dependence (*33*).

RESULTS

Laser Light Scattering Analysis of EYPC−Detergent Micellar Solutions. Figure 1 shows representative data from dynamic (A) and static (B) light scattering experiments (EYPC/cholate molar ratio = 1.2 in mixed micellar solutions at 20 °C in 0.15 M NaCl). In Figure 1A, diffusion coefficient D represents the slope of the line for each mixed micellar concentration. The linearity of $Dq(\theta)^2$ indicates that D values do not vary as functions of scattering angle. In contrast, Figure 1B illustrates the substantial angular dependence of scattered light intensity when plotted as $[R_{sample}(\theta)/R_{water}(\theta)]^{-1}$, wherein Rayleigh ratio of mixed micelles, $R_{sample}(\theta)$, is normalized by the Rayleigh ratio of water, $R_{water}(\theta)$. The linear dependence of $[R_{sample}(\theta)/R_{water}(\theta)]^{-1}$ upon $q(\theta)^2$ validates the use of eq 1 for the determination of M_{app} and $(R_g)_{app}$.

Figure 2A plots $(R_h)_{app}$ values (nanometers) over a total lipid concentration range of 1.8−10.0 g/dL for the EYPC/cholate mixed micellar system depicted in Figure 1. As total lipid concentration was decreased, $(R_h)_{app}$ values increased curvilinearly from 4 nm to approximately 16 nm. Similar apparent micellar growth patterns were observed upon dilution for all EYPC−bile salt mixtures containing cholate, and taurochenodeoxycholate, when EYPC/bile salt molar ratios were 0.6−1.2 or in the case of octyl glucoside when

[4] To calculate micellar lipid concentrations, we subtracted the intermicellar concentrations of cholate and octyl glucoside, which were approximated by their critical micellar concentrations. Estimates of these values for cholate are 0.3 g/dL (7 mM) in 0.15 M NaCl and 0.2 g/dL (5 mM) in 0.4 M NaCl (*24*), respectively, and for octyl glucoside is 0.5 g/dL (20 mM) in 0.15 M NaCl (*30*). Because the relative composition of EYPC/taurochenodeoxycholate systems in 0.15 M NaCl plotted close to the phase limit at a total lipid concentration of 0.1 g/dL (= 0.6 mM), but within the micellar phase of this system (see Table 1), we ignored the intermicellar concentration of taurochenodeoxycholate in the micellar lipid calculation since it is likely to be appreciably smaller than 0.6 mM (*24*). A slight mismatch between intermicellar and critical micellar concentrations for mixed bile salt−EYPC micelles (*31*) may introduce a small systematic error in the magnitudes of M and R_g but does not change the overall conclusions of the work.

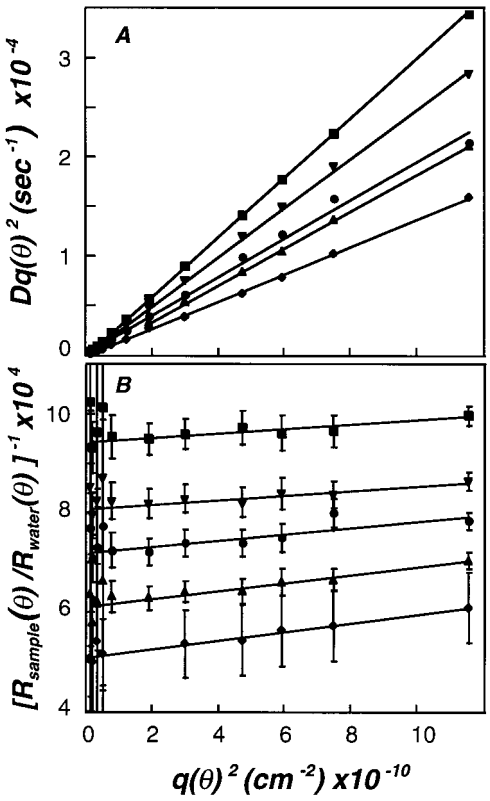

FIGURE 1: Representative dynamic (A) and static (B) laser light scattering data sets employed for the determination of M_{app}, $(R_g)_{app}$, and $(R_h)_{app}$ values. The product $Dq(\theta)^2$ (A) and the ratio $[R_{sample}(\theta)/R_{water}(\theta)]^{-1}$ (B) are plotted as functions of $q(\theta)^2$ for cholate−EYPC mixed micelles (EYPC/cholate molar ratio = 1.2, 0.15 M NaCl, pH 9, 20.0 °C) in total lipid concentrations (g/dL) of 3.6 (■), 2.9 (▼), 2.4 (●), 2.1 (▲), and 1.8 (◆). Solid lines represent linear regressions. Integer values on axes of this and subsequent figures were calculated as products of actual values multiplied by factors indicated in the axis's label.

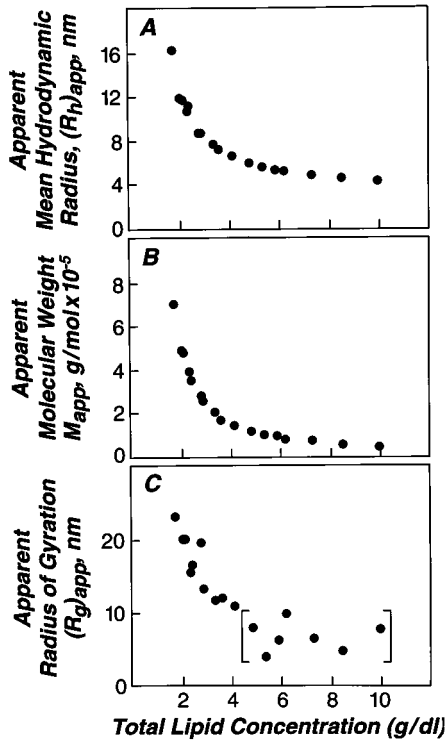

FIGURE 2: Influence of total lipid concentration on apparent mean hydrodynamic radius $(R_h)_{app}$ (A), apparent molecular weight $(M)_{app}$ (B), and apparent radius of gyration $(R_g)_{app}$ (C) of cholate−EYPC mixed micelles (EYPC/cholate molar ratio = 1.2, 0.15 M NaCl, pH 9, 20.0 °C). $(R_h)_{app}$ values were determined by quasielastic light scattering as shown in Figure 1A, whereas M_{app} and $(R_g)_{app}$ were determined by static light scattering (Figure 1B). Values of $(R_h)_{app}$, M_{app}, and $(R_g)_{app}$ each diverge with decreasing total lipid concentration. Brackets denote that values of $(R_g)_{app}$ < 10 nm could not be determined with a high degree of certainty (*18*).

the EYPC/detergent ratio was 0.13 (data not displayed). As was anticipated (*7*), when stock solutions contained considerably higher relative micellar concentrations of cholate (EYPC/cholate ≤ 0.5), dilution over the same range of total lipid concentrations did not induce any micellar growth from $(R_h)_{app}$ < 4 nm (data not displayed).

Following experimental determination of d*n*/d*C* for systems displaying strong micellar growth upon dilution (listed in Table 1), we determined M_{app} and $(R_g)_{app}$ according to eq 1 (see Figure 1B). Panels B and C of Figure 2 show the divergences of M_{app} and $(R_g)_{app}$ values, respectively, plotted as functions of total lipid concentration for the same concentration range of micellar cholate−EYPC solutions (conditions as in Figure 2A). Figure 2B shows that, with dilution, M_{app} values increase curvilinearly approximately 20-fold as total lipid concentration decreases from 10 to 1.8 g/dL. Figure 2C depicts that $(R_g)_{app}$ values increase 4-fold over the same range of total lipid concentrations, but with considerably more scatter (e.g., square bracketed) compared with Figure 2A,B. Similar increases in M_{app} and $(R_g)_{app}$ values were observed for all other EYPC-rich micellar systems as functions of decreases in total lipid concentration but not for cholate−EYPC systems when the initial EYPC/cholate molar ratios were ≤0.5 (data not shown).

Figure 3A plots the scaling ratio, $(R_h)_{app}/M_{app}^{1/2}$, derived from values plotted in Figure 2A,B as functions of total lipid concentration. Although with decreases in total lipid concentrations, both $(R_h)_{app}$ and M_{app} values increased 4- and 20-fold, respectively, while $(R_h)_{app}/M_{app}^{1/2}$ ratios remained constant with a mean value (±SD) of 0.0179 ± 0.0013 nm/(gm/mol)$^{1/2}$. Mean $(R_h)_{app}/M_{app}^{1/2} \times 10^2$ values for each EYPC-rich mixed micellar system are listed in Table 1. These values were internally consistent and comparable in magnitude despite marked variations in molecular species, total lipid concentration, and NaCl concentrations. Figure 3B displays the scaling ratios $(R_g)_{app}/(R_h)_{app}$ calculated from data plotted in Figure 2A,C as functions of total lipid concentration in the case of the EYPC/cholate system with a molar ratio of 1.2. These values show considerably more data dispersion. Points falling within the bracketed region represented points calculated using $(R_g)_{app}$ values that fell below the reliable detection limit (10 nm) of the light scattering apparatus in Figure 2C. Excluding these data, the other $(R_g)_{app}/(R_h)_{app}$ values average 1.51 ± 0.35.

Deduction of Micellar Shape. The constancy of $(R_h)_{app}/M_{app}^{1/2}$ values (Figure 3A, Table 1) if taken alone would be consistent with at least three plausible physical packing arrangements of the amphiphilic molecules (see Appendix A): (1) a dilute solution of disklike micelles as postulated previously (*7*), (2) a dilute (noninteracting) solution of random coil micelles, and (3) a semidilute (interacting) solution of random coil micelles. However, on the basis of the experimentally determined values of $(R_h)_{app}/M_{app}^{1/2}$ (Table 1), we calculate in Appendix A that the thickness of an

Table 1: Conditions and Laser Light Scattering Data for Detergent−Phosphatidylcholine Mixed Micelles[a]

detergent (D) species	EYPC/D (molar ratio)	[total lipid] (g/dL)	[NaCl] (M)	dn/dC (mL/g)	$(R_h)_{app}/M_{app}^{1/2}$ [nm/(g/mol)$^{1/2}$ × 10^2]	$(R_g)_{app}/(R_h)_{app}$
cholate	1.0	1.3−5.0	0.15	0.167	1.66 ± 0.06	1.65 ± 0.16
cholate	1.0	1.0−5.0	0.40	0.157	1.82 ± 0.06	1.68 ± 0.25
cholate	1.2	1.8−10.0	0.15	0.153	1.79 ± 0.13	1.51 ± 0.35
taurochenodeoxycholate	0.6	0.1−10.0	0.15	0.157	1.73 ± 0.33	1.66 ± 0.40
octyl glucoside	0.13	1.1−10.0	0.15	0.147	1.81 ± 0.13	1.63 ± 0.50

[a] Abbreviations: D, detergent; EYPC, egg yolk phosphatidylcholine; dn/dC, refractive index increment; $(R_h)_{app}$, apparent mean hydrodynamic radius; M_{app}, apparent molecular weight; $(R_g)_{app}$, apparent radius of gyration.

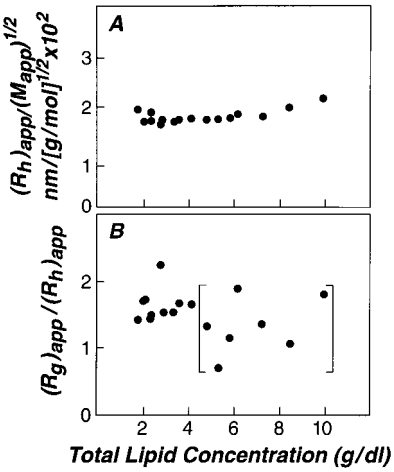

FIGURE 3: Influence of total lipid concentration on $(R_h/M)_{app}^{1/2}$ (A) and $(R_g)_{app}/(R_h)_{app}$ (B) ratios. Values are replotted from Figure 2. $(R_h)_{app}/(M)_{app}^{1/2}$ and $(R_g)_{app}/(R_h)_{app}$ values remain constant despite marked increases in $(R_h)_{app}$, M_{app}, and $(R_g)_{app}$ values with decreases in total lipid concentration (Figure 2). Brackets denote $(R_g/R_h)_{app}$ values calculated from measured $(R_g)_{app}$ values < 10 nm (Figure 2C), which could not be precisely determined (*18*).

Table 2: Relationship between Apparent and Actual Values of the Overlap Parameter When $C_L \gg \xi_p$, According to Equation A27[a]

X_o	$\Theta(X_o) = M/M_{app}$	$X_{app,o}$
0.10	1.12	0.095
0.50	1.63	0.39
1.0	2.35	0.65
2.0	4.0	1.0
5.0	9.8	1.6
10.0	21.5	2.2

[a] Abbreviations: C_L, contour length; ξ_p, persistence length; M, molecular weight; M_{app}, apparent molecular weight.

assumed disk would be close to 1 nm. This analysis takes into account the effect of excluded volume interactions between hypothetical disks, insofar as they may affect the second virial coefficient contributing to M_{app}. Therefore, a dilute solution of disklike micelles is not consistent with the $(R_h)_{app}/M_{app}^{1/2}$ values (Table 1) since the bimolecular thickness of liquid crystalline EYPC in water is at least 4 nm (*34*). Similarly as listed in Table 1, the $(R_g)_{app}/(R_h)_{app}$ ratios (Figure 3B) cluster in the vicinity of 1.5−1.7 for all compositions and not 1.1 as would be expected for disks (see Appendix A and references therein).

We examined next the hypothesis that EYPC-rich mixed micelles form locally cylindrical wormlike coils. This analysis is detailed in Appendix A (and references therein) and considers whether the model applies if the micelles formed either dilute (noninteracting) or semidilute (interacting) solutions of wormlike coils. In Appendix A, we show first that a noninteracting solution of such micelles, with reasonable diameter of $d = 4$ nm (*34*) and persistence length[5] of $\xi_p = 17$ nm, would be compatible with the observed values of $(R_h)_{app}/M_{app}^{1/2}$ and $(R_g)_{app}/(R_h)_{app}$. We then examine the effects of intermicellar interactions under two different conditions: near-dilute solutions in which individual wormlike micelles interact in a crowded environment (*14*) and semidilute solutions in which wormlike micelles become entangled with each other (*35*−*37*). For near-dilute solutions (see Near-Dilute Solution Analysis in Appendix A and Table 2), the effects of excluded-volume interactions between micelles are assessed by incorporating the second virial coefficient. We show that for two of the systems studied, EYPC/TCDC = 0.6 and EYPC/C = 1.0 (both in 0.15 M NaCl), a wormlike coil model of $d = 4$ nm and $\xi_p = 17$ nm remains consistent with our light scattering measurements because the correction introduced using the virial coefficient is sufficiently small that values of M are accurately represented by measurements of M_{app}. This is not the case for the remaining systems listed in Table 1, which instead behave as semidilute solutions (see Semidilute Solution Analysis in Appendix A) in which the light scattering data [M_{app}, $(R_g)_{app}$, and $(R_h)_{app}$] are consistent with overlapping wormlike coils. Our analysis reveals that a range of values for ξ_p and d are possible for wormlike coils in semidilute solutions. Specifically, we illustrate in Appendix A that wormlike micelles with two plausible combinations of ξ_p and d ($\xi_p = 17$ nm, $d = 4$ nm, $\xi_p/d = 4$ and $\xi_p = 38$, $d = 4.7$ nm, $\xi_p/d = 8$) may be both consistent with the light scattering data and yet correspond to contrasting sizes of micelles in semidilute solutions.

In Table 3, we show for the EYPC/cholate = 1.2 system and an assumed ratio of $\xi_p/d = 4$ that extensive micellar growth (increasing M) is required upon dilution to produce the observed values of M_{app}. Upon dilution near the micellar phase limit, these mixed micelles grow and become increasingly entangled to form a semidilute solution. Consistent with this reasoning, the inferred $(R_g)_{app}/d$ and $(R_h)_{app}/d$ (Table 3) are in excellent agreement with experiment at high dilution.

In Table 4, we show the results of an analysis of the EYPC/cholate = 1.2 system with an assumed value $\xi_p/d = 8$ instead of $\xi_p/d = 4$. In this case, extremely long micelles at high detergent concentrations could be quite compatible with the relatively small values observed for $(R_g)_{app}/d$ and $(R_h)_{app}/d$. In this case, a considerable portion of the apparent micellar growth with dilution would be due to disentangle-

[5] The micellar shape most consistent with our light scattering data is a locally cylindrical wormlike coil. As depicted in Figure 6, the wormlike micelle is characterized by diameter, d, persistence length between turns, ξ_p, and an overall contour length, C_L.

Table 3: Analysis of the EYPC/C = 1.2, 0.15 M NaCl System under the Assumption That $\xi_p/d = 4$ and $\psi = \psi^*$ [a,b]

						$(R_g)_{app}/d$		$(R_h)_{app}/d$	
$\phi \sim C_T - IMC$	M_{app}/M_c	M/M_c	$R_g°/d$	$R_h°/d$	X	predicted	measured	predicted	measured
0.097	1.2	1.4	0.5	0.6	0.14	0.5		0.6	1.2
0.059	2.5	3.1	1.0	0.9	0.29	0.9		0.9	1.0
0.045	3.8	5.3	1.4	1.2	0.31	1.3		1.1	1.5
0.033	5.5	9.2	2.2	2.6	0.52	1.9		1.4	1.8
0.026	8.3	24.5	4.6	2.9	1.40	3.2	3.3	2.0	2.2
0.021	11.5	49.0	7.2	4.3	2.2	4.1	4.2	2.7	2.8
0.018	15.6	88.0	10.1	6.0	2.9	5.0	5.0	3.0	3.0
0.015	23.0	150.0	13.6	8.0	3.4	6.0	5.8	4.0	4.0

[a] Using $d = 4$ nm and the corresponding $M_c = 3.03 \times 10^4$ g/mol. The micellar phase limit corresponds to $0.0143 < \phi < 0.0148$. [b] Abbreviations: EYPC, egg yolk phosphatidylcholine; C, cholate; ξ_p, persistence length; d, diameter; M_c, molecular weight of reference cylinder; ϕ, volume fraction of amphiphiles in micelles; IMC, intermicellar concentration; M_{app}, apparent molecular weight; $R_g°$, dilute solution value for R_g; $R_h°$, dilute solution value for R_h; X, overlap parameter; M_{app}, apparent molecular weight; $(R_g)_{app}$, apparent radius of gyration; $(R_h)_{app}$, apparent mean hydrodynamic radius.

Table 4: Analysis of the EYPC/C = 1.2, 0.15 M NaCl System under the Assumption that $\xi_p/d' = 8$ and $\psi = \psi^*$ [a,b]

					$(R_g)_{app}/d'$		$(R_h)_{app}/d'$	
$\phi \sim C_T - IMC$	$M_{app}(exp)/M_c'$	M/M_c'	$M_{app}(pred)/M_c'$	X	predicted	measured	predicted[c]	measured
0.097	0.7	100	0.9	41	1.0		0.7	1.0
		200	0.9	68	0.6		1.0	1.0
0.059	1.5	100	1.6	25	1.5		1.1	0.9
		200	1.7	41	1.6		1.5	0.9
0.045	2.3	100	2.2	19	1.8		1.7	1.3
		200	2.3	32	1.9		1.8	1.3
0.033	3.4	200	3.4	23	2.5		2.2	1.5
0.026	5.0	300	5.0	24	3.0	2.8	2.8	1.9
0.021	7.0	400	7.0	23	3.5	3.5	3.2	2.4
0.018	9.5	600	9.5	25	3.9	4.3	3.6	2.6
0.015	14.0	1000	14.0	27	4.8	4.9	4.4	3.4

[a] Using $d' = 4.7$ nm and the corresponding $M_c' = 5 \times 10^4$ g/mol in eq A26 together with the stipulation that the micelles at high volume fractions ϕ are very large compared to 1. [b] Abbreviations: exp, experimental value; pred, predicted value; other abbreviations are as described in Table 3, except where the prime denotes assignment of a different numerical value. [c] Calculated with the use of $R_h°/d' = {}^3/_8(\pi/3)^{1/2}[(M/M_c)(\xi_p/d')]^{1/2}$ together with the compilations noted in the text.

ment of long micelles, even though Table 4 does show that individual micelles would still be expected to grow themselves upon dilution. Although theoretically possible, ancillary information argues against the presence of long, entangled mixed micelles at high lipid concentrations (see below).

We note that there are caveats of potential importance with respect to the application of polymer solution properties directly to the micellar systems as we have just described. First, in addition to the micellar size and interactions considered here, changes in the micellar size distribution with concentration and composition can contribute (*38*) to the magnitude of the light scattering fluctuations (*39*, *40*). Evaluation of this contribution awaits a self-consistent thermodynamic treatment of these mixed micellar systems that incorporates intermicellar interactions. Second, because of the changing micellar size distribution, we have no straightforward means of determining solvent quality, as could be done for polymer solutions by evaluating virial coefficients. We have chosen to use polymer solution results corresponding to a good solvent regime (*41*−*43*), keeping in mind that the headgroups of all except one (octyl glucoside) of the detergents we have used are charged, and that isotropic liquid−isotropic liquid phase separations have not been reported for these systems. Third, because of the delicate noncovalent attractions that join amphiphiles into micelles, entanglements of wormlike micelles may display very different kinetic interactions from those of covalently linked polymers. These could in turn affect the diffusivities of the light scattering fluctuations that we have measured. Evaluation of each of these considerations will require additional experimental and theoretical work.

DISCUSSION

The results of this work suggest that mixed micelles composed of EYPC and two detergents of distinct molecular structure (i.e., anionic bile salts with rigid steroid backbones and nonionic octyl glucoside with a highly flexible acyl chain) may take the form of elongated locally cylindrical but flexible micelles near the micellar phase limit of the systems. This finding challenges the proposal in our earlier mixed disk model (*7*), which was based on the premise (*8*, *9*) that bile salt molecules would most efficiently solubilize PC molecules by coating the perimeters of circular PC bilayer disks. We will first reconsider the earlier laser light scattering data and proposals of Mazer et al. (*7*) in the context of the currently suggested wormlike structure for detergent−EYPC mixed micelles. On the basis of the ternary detergent−EYPC−water phase diagram, (*32*, *44*, *45*) we will address the theoretical likelihood that a wormlike mixed micellar structure presages the appearance of an intervening hexagonal (H_I) liquid crystalline phase in the transition from mixed micelles to vesicles upon dilution (*1*, *6*). We will then relate these concepts to the physiology of bile formation, which in its earliest stages involves a reversal of the serial dilution

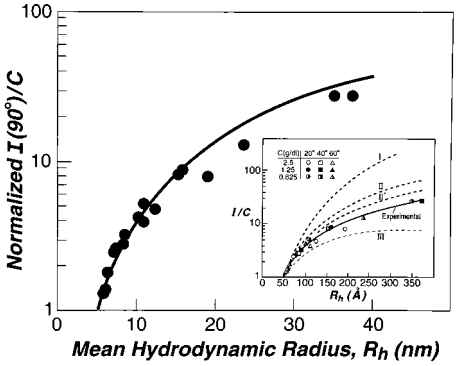

FIGURE 4: Influence of mean hydrodynamic radius, R_h, of mixed micelles on the ratio of mean scattered light intensity at 90° to micellar lipid concentration [$I(90°)/C$]. Solid circles represent data replotted from Mazer et al. (*7*). Micellar solutions were composed of taurocholate and EYPC (0.15 M NaCl, pH ~7) with total lipid concentrations ranging from 0.625 to 2.5 g/dL at temperatures of 20−60 °C. The solid curve represents the theoretical dependence of $I(90°)/C$ on R_h for a wormlike mixed micelle (see Appendix B), which provides an excellent fit to the earlier data. For normalization, we chose $\theta = 90°$ and $\alpha = 5$ nm as did Mazer et al. (*7*). Inset is a reproduction of the original Figure 7 of Mazer et al. (*7*), where I, II, II′, and III are the theoretical dependences for micellar growth as spheres, disks, polydisperse disks, and stiff rods, respectively. Inset reprinted with permission from ref 7. Copyright 1980 American Chemical Society.

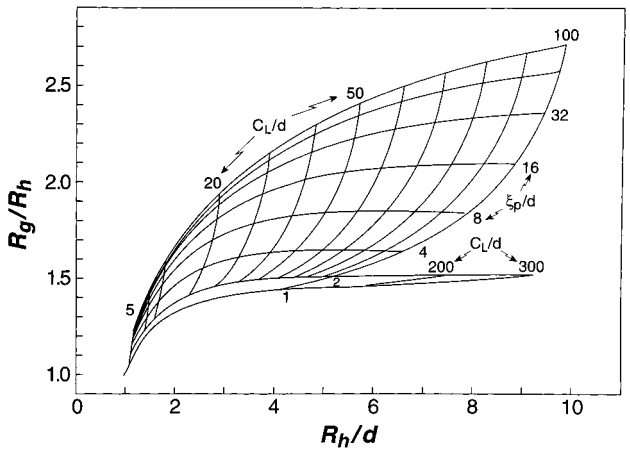

FIGURE 5: Predicted values of R_g/R_h and R_h/d for wormlike mixed micelles based on the Yamakawa and Fujii theory (*41, 47*). By use of values of R_g and R_h experimentally determined by light scattering and an independently measured value for d, the contour length C_L and persistence length ξ_p of wormlike mixed micelles in solution may be estimated graphically (see text for details).

operation on bile salt/PC (plus cholesterol) mixed micelles (*20, 21*).

Reinterpretation of Previous Light Scattering Data. Mazer et al. (*7*) deduced the most likely bile salt−EYPC mixed micellar shape by plotting mean scattered light intensity [$I(\theta)$] divided by micellar lipid concentration [$I(\theta)/C$] as functions of R_h values obtained by QLS at $\theta = 90°$ (data from ref *7* insetted in Figure 4). As demonstrated by the inset (Figure 4), the theoretical dependency of $I(90°)/C$ on R_h is distinct for spheres, disks, polydisperse disks, and stiff rods (see roman numerals in figure legend). Although Mazer et al. (*7*) noted that none of these shapes individually provided a perfect fit to their experimental data, polydisperse disks provided the closest approximation (Figure 4 inset, curve II′). Because of an earlier suggestion in the literature that bile salt and EYPC molecules packed as disklike bilayers (*8*), a comparison of micellar sizes predicted by the model of Small (*8*) and Dervichian (*9*) with the R_h values experimentally derived by dynamic light scattering (*7*) revealed that the simple disk structure was too small to account for the apparent growth. The structural and mathematical model of Mazer and colleagues (*7*) was based on the proposed equilibrium packing of the molecules in the lamellar liquid crystalline phase of bile salt−EYPC−H_2O systems (*34, 45*) where bile salts were believed to be inserted as reverse micelles into the EYPC bilayers. In the modification of the simple model, it was assumed that PC bilayers were saturated with bile salts before being cut up to form mixed micelles by extra bile salts that formed a bilayered ribbon on the perimeter of the disks. This mixed disk structure, i.e., expanded simple disk model, predicted that in addition to bile salt molecules coating the disk's perimeter, they were also incorporated into the micellar bilayers as reverse dimers with their long axes parallel to the EYPC bilayer. Interestingly, the model accurately predicted mixed micellar growth determined by QLS as functions of increasing EYPC/bile salt ratio at constant total lipid concentration (*7*) as well as increasing EYPC/bile salt ratio in micelles induced by decreasing total lipid concentration (*46*). In the absence of static light scattering data, which demonstrates herein that any disk model would be unrealistically thin, these two groups did not consider the option to make an $I(\theta)/C$ versus R_h prediction for a flexible rod or wormlike structure (see inset, Figure 4). It is salutory to find, as demonstrated by the main graph in Figure 4, that there is, in fact, excellent agreement between the original R_h data of Mazer et al. (*7*), plotted as solid circles, and the theoretical dependency of $I(\theta)/C$ versus R_h for a wormlike mixed micelle, plotted as a solid line (see details of derivation in Appendix B).

Figure 5 demonstrates graphically the relationships between light scattering measurements, R_g and R_h, and the physical dimensions of wormlike micelles, C_L and ξ_p (*41, 47*). When ancillary data provide a reasonable estimate for the value of d (e.g., $d = 4$ nm for detergent−PC micelles; see above), values of R_g and R_h may be employed to estimate corresponding values of C_L and ξ_p. For detergent−PC solutions at high dilution [i.e., $R_g \sim (R_g)_{app}$ and $R_h \sim (R_h)_{app}$], experimental values from light scattering measurements may be applied directly. However, at higher lipid concentrations at which intermicellar interactions become important, $(R_g)_{app}$ and $(R_h)_{app}$ values must first be corrected to yield corresponding values for R_g and R_h as described in Appendix A.

Molecular Model for Bile Salt−Long-Chain PC Mixed Micelles. Figure 6 proposes a schematic model for a wormlike and a globular bile salt−EYPC mixed micelle (the latter represented by a bile salt-rich fragment) and highlights their essential features. This model is consistent with accumulating evidence in the literature, which argues strongly that mixed detergent−PC micelles at low PC content are locally cylindrical objects. Employing small-angle neutron scattering (SANS), which is sensitive to short-range order, Hjelm et al. (*10*) provided evidence that EYPC-rich mixed micelles containing glycocholate (the common aminoacyl conjugate of cholate) are elongated structures with constant radii of ~2.7 nm, and subsequently these authors (*11*) used SANS to suggest that the long axes of PC molecules pack normally (i.e., perpendicular to long axes) in rodlike mixed micelles. Due to its model dependency, this radial dimension

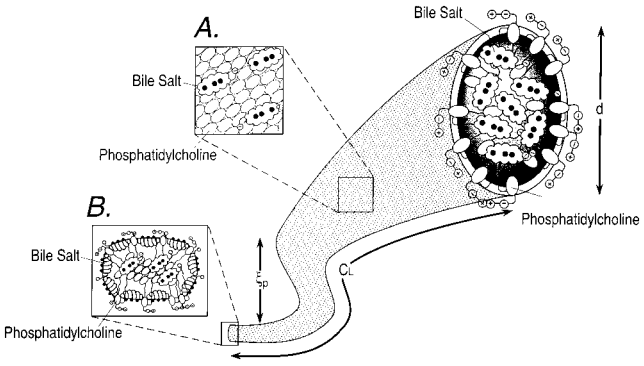

FIGURE 6: Schematic model of wormlike mixed micelles. The dimensions of the wormlike micelle are characterized by diameter, d, persistence length between turns, ξ_p, and an overall contour length, C_L. The proposed molecular packing of PC is radial with their acyl chains oriented toward the center of the wormlike mixed micelle and zwitterionic headgroups facing outward at the aqueous interface. Consequently, the micellar diameter (4 nm) is approximately twice the molecular length of a long-chain PC. Bile salt molecules both "cap" the hydrophobic ends of the mixed micelle and are dispersed randomly on the surface of the micelles (area of detail A) with their hydrophobic surfaces interacting with acyl chains of PC and their hydrophilic surfaces and ionic side chains oriented toward the aqueous continuum. Area of detail B demonstrates the globular shape of a mixed micelle at high total lipid concentrations and high bile salt-to-PC ratios, such as would occur in native bile. This particle is quasispherical with $R_h \sim 4$ nm. Upon dilution, mixed micelles grow by elongating (increasing C_L) but maintaining constant diameter to form flexible wormlike structures. Dilution induces bile salts to migrate to the intermicellar water; hence the mixed micellar PC-to-bile salt ratio increases. This wormlike particle would likely occur only at high dilution, i.e., in the intrahepatic biliary tree, especially bile canaliculi, during bile formation. (See text for further details).

is not exactly in agreement with the 2 nm length of a typical long-chain PC experimentally determined from X-ray scattering of EYPC bilayers (*34*) and hexagonal (H_I) phase rods (*32*). However, the model is in keeping with data demonstrating that PC molecules are freely diffusible within rods in the hexagonal (*48*) as well as in the cubic phase (*49*) of the ternary cholate−EYPC−H_2O systems (*44*, *45*). Based upon these observations, Figure 6 depicts PC molecules oriented radially with their hydrophobic side chains oriented toward the center of the cylinder and their zwitterionic headgroups facing the aqueous phase. To explain HPLC measurements of mixed micellar growth that were also consistent with a locally cylindrical mixed micellar structure, Nichols and Ozarowski (*12*) proposed that bile salts capped the ends of the cylinders as shown in Figure 6. Because recent surface balance studies have clearly demonstrated that dihydroxy (and by inference, trihydroxy) bile salts partition into PC monolayers with the long axis of their steroid nuclei parallel to (*50*) and not normal to (*45*) the PC−water interface, we have also introduced in Figure 6 horizontally oriented bile salts inserted into the sides of the cylinders.

The light scattering measurements and analysis in our study complement data on so-called short-range order by suggesting an overall mixed micellar structure (Figure 6). At high total lipid concentrations and mixed micellar bile salt contents, small spherocylindrical or globular mixed micelles are consistent with our measurements. Although we demonstrate in Appendix A that the same data could also be obtained on systems containing elongated, entangled mixed micelles, independent observations on similar systems

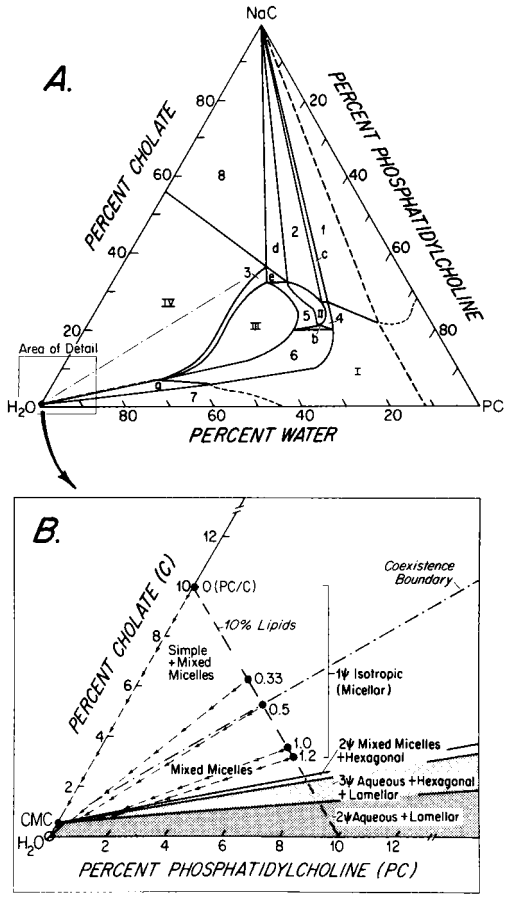

FIGURE 7: (A) Cholate (C)−egg yolk phosphatidylcholine (EYPC)−water phase diagram (*44*) with axes plotted in weights percent (pH 10.0, 20 °C, 1 atm). Solid lines represent well-defined phase boundaries, whereas dashed lines represent phase boundaries that have not been precisely determined. Roman numerals (I−IV) indicate one-phase zones, Arabic numerals (1−8) indicate two-phase zones, and letters (a−e) indicate three-phase zones. The dot at about 0.5% (w/w) on the cholate-water axis represents the critical micellar concentration (cmc) of cholate in water (~10 mM). The interrupted line (- − -) represents a coexistence boundary within the micellar zone (see below). (B) Expanded "area of detail" from the triangle. The base axis has been replotted to show weight percent (egg yolk) PC increasing from left to right, rather than weight percent water from right to left. The portions of the phase diagram represented in the area of detail are region IV, one phase (symbol ψ) which is isotropic (micellar); next to this is a sliver of region 3, containing two phases, mixed micelles plus hexagonal phase; next to this is region a, containing three phases, aqueous plus hexagonal plus lamellar; and next to this is region 7, containing two phases, aqueous plus lamellar. The micellar phase is divided by a coexistence boundary into a region containing mixed micelles plus simple micelles and a region containing mixed micelles only. The dashed line connecting the cholate and (egg yolk) PC axes represents compositions containing 10% total lipid concentrations. Arrowed lines originating at 10% lipids and directed toward the H_2O vertex represent dilution pathways of lipid compositions studied by laser light scattering in this work. The relatively low concentration of NaCl (0.15 M) employed in most of our experimental mixed micellar systems lowers the cmc of cholate to ~0.3 g/dL (*24*) and therefore slightly alters the absolute locations of the phase boundaries. [Modified from Small et al. (*44*), Cabral and Small (*6*), and Carey (*1*) with permission.]

argue against this possibility: Viscosities of concentrated (10 g/dL) bile salt−EYPC mixed micelles with compositions that plot close to the coexistence boundary (see Figure 7) do not differ substantially from water but rise dramatically near the micellar phase limit (*51*), consistent with growth of

mixed micelles as interacting wormlike structures. Moreover, recent analysis by cryo-electron microscopy failed to visualize elongated mixed micelles in concentrated bile salt-rich model biles (D. L. Gantz, D. Q.-H. Wang, M. C. Carey, and D. M. Small, unpublished observations). As total lipid concentration or mixed micellar bile salt content is reduced, our data indicate the "globular" bile salt−EYPC aggregates elongate to from wormlike mixed micelles with C_L and ξ_p dimensions (Figure 5) that are consistent with the Yamakawa−Fujii theory (*47*).

Mixed Micelle−Liquid Crystalline Phase Transition. Our proposed wormlike structure of mixed micelles near the micellar phase limit provides a possible basis for understanding the transition from mixed micelles to an intervening hexagonal (H_I) phase and then to a unilamellar vesicle (liquid crystalline) structure (*6*), which apparently occurs upon dilution of mixed bile salt−EYPC micellar systems (*7*) as reinterpreted by Cabral and Small (*6*). Figure 7A displays the ternary cholate−EYPC−water phase diagram (*45*) and Figure 7B provides in detail the representation of the aqueous-rich (≤10 g/dL total lipid concentration) fragment of the phase diagram (*1, 6*) that is best supported by available data (*52*). Compositions falling within the unshaded region of Figure 7B are micellar and correspond to zone IV of Figure 7A. The micellar zone is bisected by a dot-dashed line (shown in Figure 7A,B), which represents the coexistence boundary between simple micelles plus mixed micelles and mixed micelles alone where a divergence in micellar size (Figure 2) commences (*7*). Due to their differing symmetries, the isotropic phase (zone IV), the hexagonal phase (zone III), and the lamellar phase (zone I) must all be joined pairwise by at least three regions of two-phase coexistence, assuming that all single phase regions have now been identified. In turn, these two-phase regions must form the borders of at least one triangle, the vertexes of which specify the compositions of three phases coexisting in equilibrium (i.e., a triangle that joins zones I, III, and IV). A number of geometries can satisfy these constraints. One possibility is depicted in Figure 7A: The isotropic vertex of the three-phase triangle corresponds to a very dilute solution, as suggested on the basis of X-ray scattering data gathered at low total lipid concentrations (*1, 6, 52*). Figure 7B shows a two-phase region (lightly shaded) in which the hexagonal phase coexists with mixed micelles is directly adjacent to the micellar zone (*1, 6, 52*). Under this scenario, this two-phase region would adjoin a three-phase region containing hexagonal phase, a lamellar liquid crystalline phase, and aqueous cholate monomers (zone a in Figure 7A, intermediate shading in Figure 7B). The heavily shaded two-phase region in Figure 7B (zone 7 in Figure 7A) would contain only a lamellar liquid crystalline phase in the metastable form of unilamellar vesicles, aqueous cholate monomers in concentrations below their critical micellar concentration (cmc, shown as a closed circle on the cholate axis in Figure 7B), and extremely dilute PC monomers. Another less likely possibility not pictured in Figure 7 is that the isotropic vertex of the three-phase triangle is located at a higher total lipid concentration (i.e., away from the H_2O vertex) as originally proposed by Small et al. (*45*) and which formed the basis of the phase equilibria data available to Mazer et al. (*7*) prior to their revision by Small (*52*). In this case, a dilution path from the mixed micellar phase could directly enter the lamellar phase without traversing a three-phase region. Additional experimental evidence will be needed to distinguish whether this possibility could be correct under certain circumstances, bearing in mind that such phase relations could occur in systems containing different molecular species of detergents, phospholipids, and experimental conditions.

In the present systems, it is also possible that the micellar size increases sufficiently so as to facilitate a transition to a partially ordered (i.e., dilute hexagonal, H_I) coexisting phase, as suggested (*6*). In support of this possibility, statistical mechanical models of semiflexible spherocylinders with excluded-volume interactions show that the volume fractions of coexisting isotropic and hexagonal phases (*53−56*) decrease strongly with increasing contour length-to-diameter or persistence length-to-diameter ratios. We note that in solutions containing particles of fixed dimensions, a transition to a partially ordered phase occurs upon increasing volume fraction. Such a transition is also consistent with what is observed for the phase equilibria system studied here (*32*), where at higher lipid volume fractions there is a phase transition from zone IV (micellar) to zone III (H_I) (Figure 7A). In contrast, we have performed the present light scattering measurements on micellar systems where growth also occurs, but upon decreasing the overall lipid volume fraction (Figure 7B). Arrowed lines in Figure 7B represent the dilution paths studied in this work by QLS and static light scattering. Clearly only the detergent is present with EYPC/cholate = 0, and as anticipated, no micellar growth occurs upon dilution, and in contrast only monomers are present below the cmc (Figure 7B). Dilution paths containing EYPC/cholate molar ratios of 0.33 fall almost entirely within the region of the micellar zone in which simple and mixed micelles coexist and for which we observed no micellar growth experimentally. No growth was anticipated because, as was noted earlier by Mazer et al. (*7*), the proportions of mixed micelles increase relative to simple micelles, and hence no change occurs in mixed micellar composition nor in size measured by QLS. When the EYPC/cholate molar ratio = 0.5, which plots close to the coexistence limit (Figure 7B) due to the relatively high cholate concentration, we were unable to discern significant micellar growth with dilution prior to loss of the light scattering signal. In contrast, compositions containing EYPC/cholate molar ratios > 0.5 (1.0−1.2) contained only mixed micelles (Figure 7B), and these grew upon dilution due to loss of bile salts from the mixed micelles to maintain the intermicellar monomer concentrations (*7*). This dilutional loss of bile salts relative to EYPC molecules from mixed micelles at the higher EYPC contents (EYPC/cholate molar ratios of 1.0 and 1.2) markedly reduces cholate content in the mixed micelles and, as we observed, resulted in dramatic increases in R_h values (Figure 2A). Indeed, cryo-transmission electron microscopy of an cholate−EYPC−water system with a composition (EYPC/cholate = 1.1, total lipid concentration = 1 g/dL), (*13*) that plots near the micellar zone (Figure 7B) demonstrated rodlike objects of ∼200−300 nm in length and ∼5 nm in width.

Physiological Correlations. It is known now that long-chain PCs are secreted as unilamellar vesicles into the canalicular spaces between liver cells by mechanisms independent of bile salt secretion (*57*). We have suggested

elsewhere (*20*) that in the initial formation of bile from interaction of bile salt molecules with these vesicles, the first micelles that are formed in such a bile salt−PC mixture would be wormlike objects. From in vitro model studies, this occurs only when the secreted bile salt concentration attains its critical micellar concentration in the proximal biliary tree (*20*). On the basis of the similar findings for octyl glucoside−EYPC mixed micelles in the present work, it is anticipated that similar wormlike mixed micelles should occur during bile formation in crustacea where medium-length acyl chain detergents with dipeptidyl headgroups rather than steroid detergents with flexible side chains solubilize long-chain PC (*2*). It is important to note that we have not examined herein the influence of cholesterol incorporation on mixed micellar structure and that solubilization of biliary cholesterol may alter or even prevent formation of wormlike structures depending upon its absolute and relative concentrations.

Although our light scattering data strongly suggest that biologically relevant wormlike mixed micelles may form in the presence of detergents with quite distinct (i.e., steroid and acyl chain) molecular structures, "micellar" solubilization of long-chain PC is known to occur by other mechanisms. An important example is recombinant high-density lipoprotein particles, in which apolipoprotein AI complexes with long-chain PC (or other natural phospholipids), and apolipoprotein AI−EYPC recombinants have been shown by several experimental methods to form bilayer PC disks stabilized by apolipoprotein AI at their edges (*58*). Most recently, van Antwerpen et al. (*59*) have employed cryo-electron microscopy to demonstrate disks of thickness of 5.1 ± 0.1 nm and diameter 18.8 ± 3.5 nm upon reconstitution of high-density lipoproteins with 1-palmitoyl,2-linoleoyl-PC, cholesterol, and apolipoprotein AI.

In summary, it appears that the solubilization of long-chain PCs in bile of both vertebrates and invertebrates most likely involves packing of PC together with steroid (or straight-chain) bile salt molecules into globular rods or elongated wormlike particles depending upon the PC/detergent ratio. In contrast, the apolipoprotein−PC micelles of blood that form the basis of nascent high-density lipoprotein particles are clearly disklike in structure. It remains to be determined whether physiological advantages accrue from these dissimilar modes of packaging PC into small soluble particles in the major biological fluids.

APPENDIX A: ANALYSIS OF POSSIBLE MIXED MICELLAR SHAPES

(1) Disk. Although we are not aware of a precise expression for R_h of a disk as a function of fixed overall thickness (t) and variable radius (r), R_h may be estimated by considering a disk a limiting case of an oblate ellipsoid with semimajor axis r and semiminor axis $t/2$ (*60*):

$$R_h = (t/2)((2r/t)^2 - 1)^{1/2}/\tan^{-1}[((2r/t)^2 - 1)^{1/2}] \quad \text{(A1)}$$

For $r \gg t$, this expression simplifies to $R_h = 2r/\pi$. On the other hand, the molecular weight of the fixed thickness disk is given by $M = \pi r^2 t N_a \rho$, where ρ is the mass per unit volume of lipid within the micelle. Clearly, the ratio $R_h/M^{1/2}$ is constant for a disk of a given t, and t may be expressed as

$$t = [(\pi^3/4)\rho N_a(R_h/M^{1/2})^2]^{-1} = [(\pi^3/4)\rho N_a]^{-1}(M/R_h^2) \quad \text{(A2)}$$

For an initial estimate of t, we assume $M \sim M_{app}$ and $R_h \sim (R_h)_{app}$. Using $R_h/(M)_{app}^{1/2} = 0.018$ nm/(g/mol)$^{1/2}$ from Table 1 and assuming $\rho = 1$ g/mL for mixed micelles, we calculate that $t \sim 0.7$ nm. As explained in the text, this value is not consistent with a PC bilayer that forms the basis of the simple or mixed disk models for mixed bile salt−EYPC micelles (*7*−*9*).

In solutions that are not dilute, the presence of attractive or repulsive intermicellar interactions such as those due to van der Waals forces, surface charges, or excluded volume affect the intensity of scattered light, so that $M_{app} \neq M$. In particular, net repulsive intermicellar interactions lead to $M > M_{app}$. We now consider whether such an effect could be large enough, in the current solutions, to increase the value of M appropriate for use in eq A2, so that t could be ≥4 nm. In this analysis, we defer consideration of intermicellar interactions on R_h. For the marked growth of presumed mixed disk micelles near the phase limit, we assume electrostatic repulsions to be effectively screened, since the solvent Debye length of <1 nm is at least 10 times smaller than what the mean intermicellar (center−center) spacing would be if the micelles were disks. Accordingly, we restrict our analysis to the influence of excluded volume interactions on the intensity of scattered light. We do so at the level of the second virial coefficient A_2, with the use of the approximation

$$M/M_{app} = 1 + 2A_2cM + ... \quad \text{(A3)}$$

where c is the micellar concentration (w/v).

The use of eq A3 for the present case of micellar solutions may be justified as follows: For a single-component solute comprising particles of fixed size, A_2 would be the coefficient of the c^2 term in the near-dilute solution expansion of the osmotic pressure $\pi = RT[(c/M) + A_2c^2 + A_3c^3 + ...]$. For our present estimate, however, we use A_2 and c in eq A3 in a hypothetical sense to describe the light scattered by micellar particles which are present at concentration c, while regarding both A_2 and M to themselves be functions of c. In doing so, we do not consider the following points, which fall beyond the scope of the current study: (i) From a thermodynamic standpoint, the present systems contain not one but two solute components. Consequently, the relationship between the intensity of the light scattered in the forward direction and chemical potential derivatives [e.g., $(\partial\pi/\partial c)_{T,p} = RT/M_{app}$ in eq A3] is more complex than that employed herein (*39*, *40*). (ii) The present experimental systems contain a size distribution of micelles that varies with detergent and surfactant concentration and composition. Whereas for a solution containing just one solute amphiphile component, the intensity of the forward scattered light can still be used to deduce $(\partial\pi/\partial c)_{T,p}$, the quantity $(\partial\pi/\partial c)_{T,p}$ here implicitly incorporates the change in micellar size distribution as a function of c. In such a case it is not clear, a priori, that eq A3 is appropriate for analysis of the light scattering data. Several groups have shown that interactions between micelles or other reversibly associating solute species can potentially influence the size distribution (*61*−*66*). (iii) Even if intermicellar interactions were to have a negligible effect on the

micellar size distribution, polydispersity is expected to contribute terms of order c^2 to eq A3 (*38*), which we neglect.

For A_2, we have used the expression given by Isihara and Hayashida (*67, 68*) for a right circular cylinder:

$$A_2 = 4VN_a/M^2\{^1/_4[1 + ((1 + x)(1 + \pi x)/2x)]\} \quad \text{(A4)}$$

in which V is the micellar volume and $x = a/2b$, where a is the disk (i.e., cylinder) radius and b is the disk half-thickness.

Using eq A4, we can write

$$(2A_2cM)_{disc} = \pi\phi x[1 + (1/x)(1 + 3/\pi) + 1/(\pi x^2)] \quad \text{(A5a)}$$

$$\sim \pi\phi x \text{ for large } x \quad \text{(A5b)}$$

where $\phi = c\bar{v}$ is the volume fraction of amphiphiles in micelles (i.e., excluding the intermicellar bile salt volume fraction) and $\bar{v} = (VN_a/M)$ is the partial specific volume of the lipids, assumed to be the same as that of the micelles. To evaluate eq A3 using eq A5 it is convenient to normalize M using a quantity defined as M_c, the molecular weight of a cylinder of lipid having diameter $2b$ and height $2b$; $M_c = (2\pi b^3)N_a/\bar{v}$, so that $(M/M_c)_{disc} = 4x^2$ and

$$(M/M_{app})_{disc} = 1 + \phi\{(\pi/2)(M/M_c)_{disc}^{1/2} + (3 + \pi) + 2((M/M_c)_{disc})^{-1/2}\} \quad \text{(A6)}$$

Using $2b = 4$ nm and $\bar{v} = 1$ cm^3/g, we find $M_c = 3.0 \times 10^4$g/mol. Writing $(M/M_{app})_{disc} = (M/M_c)_{disc}(M_c/M_{app})$ and solving for $(M/M_c)_{disc}$, neglecting virial coefficients beyond the second and neglecting $[(M/M_c)_{disc}]^{-1/2}$, we obtain $(M/M_c)_{disc} = (M_{app}/M_c)\{(1 + (3 + \pi)\phi + z^2)^{1/2} + z\}$, where $z \equiv (\pi\phi/4)(M_{app}/M_c)^{1/2}$. To linear order in ϕ this gives

$$(M/M_c)_{disc} = (M_{app}/M_c)\{1 + \phi\{((3 + \pi)/2) + (\pi/4)(M_{app}/M_c)^{1/2}\} + \text{terms of order } \phi^2\} \quad \text{(A7)}$$

Equation A7 is convenient for evaluating M using the experimental values of M_{app}. We find for each system studied that $(\pi\phi/4)(M_{app}/M_c)^{1/2}$ is below 0.1 and is near or below 0.05 in the region of apparent micellar growth. At or near the micellar phase limit, the term $\phi[(3 + \pi)/2]$ ranges up to about 0.05, although for the higher concentrations studied it can be as high as 0.3. Therefore, under the hypotheses that (i) the micelles are disklike, and (ii) eq A3 can be applied, consideration of excluded volume interactions would not significantly increase the values of M from those we infer by using $M \approx M_{app}$.

From eq A2 and using $M/M_{app} = 1.2$ (which exceeds the largest value calculated from eq A7 near the dilution limit), we may conclude that R_h would have to be smaller than $(R_h)_{app}$ by a factor of 2.2 in order to be consistent with circular disks having a thickness of at least 4 nm. Such a large effect would be implausible on the basis of the following considerations: An estimate of the collective diffusion coefficient $D_c(\phi)$ of a colloidal or polymer suspension can be made using $D_c(\phi)/D(0) = R_h(0)/(R_h)_{app} \approx [\eta(0)/\eta(\phi)][(\partial\pi/\partial\phi)/(\partial\pi/\partial\phi)_0]^{1/2}$, where $(\partial\pi/\partial\phi)_0$ is the limiting value of $(\partial\pi/\partial\phi)$ as ϕ approaches 0 and $\eta(\phi)$ is the viscosity of the suspension (*69, 70*). Evaluation of $(\partial\pi/\partial\phi)$ to linear order in ϕ using eqs A3 and A5 and $\eta(\phi)$ for a suspension of disks according to Boek et al. (*71*) reveals the change for solutions near the dilution limit to be well below 1%.

In summary, the estimates given above suggest that neither M_{app} nor $(R_h)_{app}$ would be significantly affected by excluded volume intermicellar interactions between disklike micelles. In turn this supports our initial conclusion, i.e., that the apparent disk thickness $t = 2b$, as calculated from $(R_h)_{app}/M_{app}^{1/2} = 0.018$ nm/(g/mol)$^{1/2}$, is too small to be consistent with disklike micelles. Additional evidence derives from the observation that the experimental values of the $(R_g)_{app}/(R_h)_{app}$ ratio are not compatible with those to be expected for a disk. To determine R_g/R_h ratios for a disk, we derive R_g according to the definition $R_g^2 = \int r^2\, dM/\int dM$ (*29*). For a flat disk of circular cross-section having radius r and uniform thickness t, this gives

$$R_g^2 = r^2/2 + t^2/12 \quad \text{(A8)}$$

which simplifies to $R_g = r/\sqrt{2}$ for a disk with $r \gg t$. By combining the simplified forms of eqs A1 and A8, we obtain $R_g/R_h = (\pi/2)\sqrt{2} = 1.11$. In contrast, the experimentally determined values of $(R_g)_{app}/(R_h)_{app}$ were near or above 1.5 (Table 1) and are not consistent with $(R_g)_{app}/(R_h)_{app} = 1.1$ (neglecting weighting for micellar dispersity). In this analysis, we note that the above considerations did not address the influence of polydispersity or intermicellar interactions on R_g and R_h.

(2) Wormlike Coil. For illustrative purposes, a random macromolecular wormlike coil (*72*) can be represented as a large number (N) of small spherical segments connected by their centers and oriented randomly. If interactions between nonadjacent spheres are neglected, the R_h of such a coil is proportional to $N^{1/2}$ (*73*). Since the molecular weight M is proportional to N, the ratio $R_h/M^{1/2}$ is constant despite growth in the coil by increasing N. Nevertheless, the numerical value of the $R_h/M^{1/2}$ ratio will be quite different for a random coil with cross-sectional diameter ≥ 4 nm than it would be for a disk of thickness ≥ 4 nm. Our experimental finding that $R_h/M^{1/2}$ is approximately constant (Table 1) and has a value that is not consistent with disklike micelles suggested, as was discussed in abstracts of the present work (*18, 20*), that the micelles may take the form of random coils. Concurrent and subsequent work utilizing neutron scattering (*10, 11, 74*−*76*), electron microscopy (*3, 13*), gel chromatography (*12*), and light scattering (*14, 74*−*76*) provide strong evidence that locally cylindrical but flexible micelles are present in solutions similar to those studied here.

A quantitative comparison of this hypothesis with the present light scattering data, however, is significantly complicated by the presence of intermicellar interactions. Should the proposed wormlike micelles interact so as to become entangled, they may cross over to become a "semidilute" solution in which M_{app}, $(R_g)_{app}$, and $(R_h)_{app}$ would no longer represent single particle characteristics but would instead reflect the osmotic compressibility $\partial\pi/\partial c = RT/M_{app}$, the static correlation range $\xi_S = (R_g)_{app}/\sqrt{3}$ and the hydrodynamic correlation range $\xi_H = kT/(6\pi\eta D_{app}) = (R_h)_{app}$. Indeed, the well-documented characteristics of solutions of flexible polymers, when they cross over from independent linear polymers to form semidilute solutions, exhibit qualitative features similar to those shown by the present data. First, $\partial\pi/\partial c$ shows a marked increase (i.e., M_{app} decreases) for

concentrations c approaching and exceeding an overlap concentration c^*, while both ξ_S and ξ_H decrease concomitantly. Second, for $c > c^*$, the quantity $(\xi_S^2/RT)(\partial\pi/\partial c)$ is independent of c and polymer size under a variety of conditions (*42*). As noted above, the quantity $(\xi_H^2)(\partial\pi/\partial c)$ is also expected to be only a weak function of concentration in polymer solutions. Since $(\xi_S^2/RT)(\partial\pi/\partial c) = {}^1/_3(R_g)_{app}^2/(M_{app})$, and we find $(R_h)_{app}^2/(M_{app})$ and $(R_g)_{app}/(R_h)_{app}$ to be approximately constant, these expectations indeed correspond to our findings. For the present, two-solute-component micellar system, it should be noted that since the micelles appear to become larger upon dilution, it is not clear at the outset whether c/c^* will be found to increase or decrease with dilution. This is because the effective value of c^* can itself decrease with dilution due to increasing micellar size. We also note that over the past two decades, a number of other micellar solutions have also been found to exhibit the properties of dilute and semidilute solutions of linear polymers (*65, 77*−*81*).

We therefore consider our data in terms of three alternative possibilities for locally cylindrical micelles that neglect polydispersity: (1) dilute solutions of noninteracting micelles, (2) near-dilute solutions in which use of the second virial coefficient is sufficient to estimate M from M_{app}, as analyzed by Egelhaaf and Schurtenberger (*14*), and (3) semidilute solutions of entangled micelles. We point out that analysis of alternative (3) is similar to the analysis of semidilute solutions of giant, polymer-like reverse micelles by Schurtenberger and Cavaco (*35*−*37*) and by Jerke et al. (*82*). Whereas their analysis assumes a power-law dependence of micellar size upon concentration, our analysis differs because we have not assumed specific concentration dependence.

(1) Dilute Solution Analysis. We begin by showing that the ratio of R_g to R_h to be expected for noninteracting random coils is near 1.5, close to the observed values (Table 1) in the region of rapidly growing micellar sizes. This can be outlined as follows: the dimensions of a wormlike coil are characterized by radius r, persistence length ξ_p, and contour length C_L. In these terms, $M = \pi r^2 \rho C_L N_a$. In the limit where $C_L \gg \xi_p$ (i.e., a tightly coiled "worm"), the Yamakawa and Fujii theory (*41*, *47*) relates R_h to C_L and ξ_p according to

$$R_h = {}^3/_8(\pi/3)^{1/2}(C_L\xi_p)^{1/2} \tag{A9}$$

so that

$$\xi_p = {}^{64}/_3\rho r^2 N_a (R_h/M^{1/2})^2 \tag{A10}$$

The radius of gyration of a wormlike coil is given by (*41*)

$$R_g = (C_L\xi_p/3)^{1/2} \tag{A11}$$

Combining equations A9 and A11 yields $R_g/R_h = 8/(3\pi^{1/2}) = 1.5$.

Equation A10 shows that for noninteracting random coils, the experimental values of $(R_h/M^{1/2})^2$ are directly proportional to ξ_p, provided that $C_L \gg \xi_p$. Using the experimental value $R_h/M^{1/2} = 0.018$ nm/(g/mol)$^{1/2}$, $\rho = 1$ g/cm^3, and $r = 2$ nm, we obtain the estimate $\xi_p = 17$ nm. Such a value is consistent with observations for other polymerlike micelles, including those deduced by Egelhaaf and Schurtenberger (*14*) for bile salt−EYPC systems. As noted above, such an analysis neglects corrections to M_{app} and $(R_h)_{app}$, which arise from intermicellar interactions and from polydispersity. Moreover, eqs A9 and A10 both need considerable correction when C_L is comparable to ξ_p and neglect the influence of excluded volume and other intermolecular interactions on the size of the coil. Nevertheless, this estimate does suggest that the present micelles may take the form of random wormlike coils.

(2) Near-Dilute Solution Analysis. To consider the effects of intermicellar excluded volume interactions for near-dilute solutions, our method is first to derive suitable expressions for M/M_c as functions of M_{app}/M_c, consistent with a given assumed shape, where $M_c = \pi d^3 N_a/4\bar{v}$ is the molecular weight of a reference cylinder of lipid, having both diameter d and height d for algebraic convenience. We can then use the measured M_{app} together with a reasonable value of d to infer M/M_c. Since we can express both R_g/d and R_h/d in terms of M/M_c, we can thereby compare the measured R_g and R_h with the predictions for M/M_c so derived.

Following Egelhaaf and Schurtenberger (*14*), we neglect the influence of intermicellar interactions on R_h and R_g, but we again use eq A3 to evaluate the influence of excluded volume interactions on M/M_{app}. We first consider the case of straight rods (i.e., spherocylinders with long persistence length compared to the rod length) and then flexible, locally cylindrical micelles.

(a) Examination of the First-Order Effect of Intermicellar Interactions on the Straight Rod Hypothesis. As a model for an inflexible micelle ($\xi_p \gg C_L$), we use a rigid rod of length L and diameter d, for which

$$\begin{aligned}(A_2)_{rod} &= (N_A V/M^2)(L/d)\\ &= (N_A V/M^2)(M/M_c)\end{aligned} \tag{A12}$$

Substitution of eq A12 into eq A3 gives, neglecting third and higher-order virial coefficients

$$(M/M_c)_{rod} = (M_{app}/M_c)[1 - 2\phi(M_{app}/M_c)]^{-1} \tag{A13}$$

From eq A8 applied for constant r and varying t, one obtains for a rod

$$(R_g/d)^2_{rod} = 1/8 + (1/12)(M/M_c)^2 \tag{A14}$$

For R_h of a cylinder, we use

$$(R_h)_{rod} = t/2\{(1 - x^2)^{1/2}/\ln[(1 + (1 - x^2)^{1/2})/x]\} \tag{A15}$$

where $x = d/t[1 + (0.37)(t - d)/t]$ (*83*, *84*). It is noteworthy that R_h/d from eq A15 can also be written in terms of $(M/M_c) = t/d$.

We have examined each of our experimental systems using eqs A13−A15. At the higher lipid concentrations assayed (volume fractions 5−10%), the predicted R_g and R_h are, in general, smaller than the observed values $(R_g)_{app}$ and $(R_h)_{app}$. Near the micellar phase limit, however, this comparison is sensitive to d, the assumed micellar diameter. For the TCDC−EYPC system, we find straight rods having diameter $d = 4$ nm, with the associated $M_c = 3.03 \times 10^4$ g/mol, yield reasonable agreement between predicted and measured R_g and R_h values. This suggests that this system, which

demonstrated the lowest micellar phase limit of those examined (Table 1), may indeed contain rodlike micelles. For each of the other four systems, reasonable values of d can be found that bring predicted and apparent R_g and R_h into agreement for one or two of the measured concentrations, but not for the others. Thus the dilution dependence of $(R_g)_{app}$ and $(R_h)_{app}$ does not seem to match that calculated in the above manner for rods.

The above-described calculations for rods did not consider the influence of intermicellar and hydrodynamic interactions on R_g and R_h. For the TCDC−EYPC system, we expect such corrections to be small, since M/M_{app} ranges up to only 1.12. For the other systems, however, M/M_{app} calculated from eq A13 is quite large near the micellar phase limit, ranging from 1.4 for the EYPC/C = 1.0, 0.15 M NaCl system to 3.1 for the EYPC/C = 1.2, 0.15 M NaCl system. Given these large M/M_{app} values, one cannot reject the straight rod hypothesis for the latter systems without significant further analysis. Nevertheless, given recent light scattering and neutron scattering data consistent with flexible rodlike micelles (*10, 11, 14, 76*), we have focused our examination on the influence of such interactions on the flexible coil hypothesis.

(b) Examination of the First-Order Effect of Intermicellar Interactions on the Coil Hypothesis. We first examine the second virial coefficient A_2 appropriate for flexible coils, by using (*41*)

$$A_2 = 4\pi^{3/2}N_a(R_g^3/M^2)\psi \tag{A16}$$

where ψ is defined as the interpenetration function. ψ has been calculated to approach the value $\psi^* = 0.27$ (*43, 85*) for $\xi_p/C_L \ll 1$ in a good solvent (*42*). As before, we substitute the expression for A_2 in eq A16 into eq A3 to obtain

$$(M/M_{app})_{coil} = 1 + 2(4\pi^{3/2}\psi)(cN_a/M)R_g^3 + ...$$
$$= 1 + 8\pi^{3/2}\psi(R_g^3/V_{micelle})\phi + ... \tag{A17}$$

where $V_{micelle}$ denotes the volume of an individual micelle, and we have neglected polydispersity. When we define $M_c = (\pi d^3/4\bar{v})N_a$ as a convenient reference molecular weight, use $V_{micelles} = (\pi d^2/4)C_L$, and note that $C_L/d = M/M_c$, we obtain

$$(M/M_{app})_{coil} = 1 + 32\pi^{1/2}\psi(M_c/M)(R_g/d)^3\phi + ... \tag{A18}$$

We employ the approximation $(R_g/d)^2 = (C_L/d)(\xi_p/d)(1/3) = (M/M_c)(\xi_p/d)(1/3)$ appropriate for $C_L \gg \xi_p$, neglecting intracoil interactions, in eq A18 to obtain

$$(M/M_{app})_{coil} = 1 + (32\pi^{1/2}/3^{3/2})\psi^*(M/M_c)^{1/2}(\xi_p/d)^{3/2}\phi + ... \tag{A19}$$

As before, we truncate eq A19 after the terms shown, write $M/M_{app} = (M/M_c)(M_c/M_{app})$, and solve for M/M_c to obtain

$$(M/M_c)_{coil} = (M_{app}/M_c)_{coil}\{(1 + (y/2)^2)^{1/2} - (y/2)\}^{-2} \tag{A20}$$

where $y \equiv (32\pi^{1/2}/3^{3/2})\psi^*(M_{app}/M_c)^{1/2}(\xi_p/d)^{3/2}\phi$ giving

$$(M/M_c)_{coil} = (M_{app}/M_c)_{coil}\{1 + y + \text{terms of order } y^2\} \tag{A21}$$

Consulting the definition of y and eq A7, we note that the functional dependencies of M/M_c on M_{app}/M_c are quite similar in the disk and the flexible coil cases. However, the deviation of M from M_{app} is much larger under the flexible coil hypothesis, as can be seen by substituting typical values of $M_{app}/M_c = 25$ and $\phi = 0.01$ found for three of the five systems we studied (EYPC/C = 1.0, 0.4 M NaCl; EYPC/C = 1.2, 0.15 M NaCl; and OG) near the micellar phase limit, and using our previous estimate $\xi_p = 17$ nm together with $d = 4$ nm, we find $y \approx 1$ and $M/M_{app} \approx 2$. In the two other systems, the quantity y appearing in eq A21 is small compared with 1 (EYPC/C = 1.0, 0.15 M NaCl) or very small (<0.1) (EYPC/TCDC = 0.6, 0.15 M NaCl). In the latter case, the micellar dilution limit occurs below $\phi = 0.0012$, a factor of ~10 lower than for the other systems. For these two detergent−EYPC systems, therefore, consideration of intercoil excluded volume interactions does not significantly alter the inferred value of M, and presuming that R_h also does not change significantly, the light scattering data remain consistent with wormlike coils. In contrast, y is close to 1 for the other three systems, suggesting higher order terms cannot be neglected in eq A17. We therefore consider the semidilute solution case.

(3) Semidilute Solution Analysis. To address this possibility, following the work of Schurtenberger and coworkers, we use evidence based upon theoretical and experimental studies of light scattering from semidilute solutions of linear, flexible polymers of known molecular weight (*35−37, 86−94*). In particular, we shall compare our data to the work of Ohta, Oono, and co-workers, who express the degree of overlap or entanglement of such polymers in terms of the quantity $X = {}^{16}/_{9}A_2cM$, where we have neglected the polydispersity, which they include. We use eq A16 for A_2 to obtain

$$X = {}^{64}/_{9}\pi^{3/2}\psi(R_g^3/V_{micelle})\phi$$
$$X = {}^{256}/_{9}\pi^{1/2}\psi(M_c/M)(R_g/d)^3\phi \tag{A22}$$

Again, our strategy is to obtain a suitable relationship between M/M_c and M_{app}/M_c. Ohta and Oono (*87*) have developed a theoretical expression for the osmotic pressure π of semidilute polymer solutions in terms of X using renormalization group techniques. The osmotic compressibility $(\partial\pi/\partial c)_T$ corresponding to their expression for π is given by (*86, 94*)

$$(M/N_AK_BT)(\partial\pi/\partial c)_T = 1 + {}^1/_8[9X - 2 + 2(1/X)\ln(1 + X)]\exp\{{}^1/_4[(1/X) + (1 - (1/X^2))\ln(1 + X)]\}$$
$$\equiv \Theta(X) = (M/M_{app}) \tag{A23}$$

where we use the identity $(1/N_AK_BT)(\partial\pi/\partial c)_T = (1/M_{app})$, and in which we neglect polydispersity. Equation A23 has been found to give an accurate representation of the intensity of scattered light [proportional to $(\partial\pi/\partial c)^{-1}$] over a broad range of dilute and semidilute concentrations of solutions of linear polymers (*86, 95*).

Evaluation of eq A23 requires determination of X in eq A22. For micellar systems, however, neither M, R_g, nor A_2 can be obtained directly from the light scattering data in semidilute solutions. Nevertheless, one can proceed as follows: The dilute solution value of R_g for semiflexible coils, appropriate for evaluation of X, can be written in terms of the contour length C_L, the persistence length ξ_p, and the diameter d (*41, 77, 81, 96*):

$$R_g^2 = C_L^2\{(1/3w) - (1/w^2) + (2/w^4)[w - 1 + \exp(-w)]\} + (d^2/8) \quad \text{(A24)}$$

where $w \equiv C_L/\xi_p$. Using $C_L/d = M/M_c$, we obtain

$$[g(M/M_c, \xi_p/d)]^2 \equiv (R_g/d)^2$$

$$= {}^1/_3(M/M_c)(\xi_p/d) - (\xi_p/d)^2 + 2(M/M_c)^2(\xi_p/d)^4\{(M/M_c)(\xi_p/d)^{-1} - 1 + \exp[-(M/M_c)(\xi_p/d)^{-1}]\} + {}^1/_8 \quad \text{(A25)}$$

Note that the first term on the right side of eq A25 is the expression used above to obtain eq A19. By using eqs A22, A23, and A25, we have

$$(M_{app}/M_c) = (M/M_c)\{\Theta(X)\}^{-1} = (M/M_c)\{\Theta[\delta\phi(M/M_c)(g(M/M_c, \xi_p/d))^3]\}^{-1} \quad \text{(A26)}$$

where $\delta \equiv {}^{256}/_9\pi^{1/2}\psi = 13.6$ for $\psi = \psi^* = 0.27$. In so doing we neglect considerations of the radius of gyration expansion due to intercoil interactions, together with the corresponding effect on ψ (*41, 43*), and we neglect the contour and persistence length dependence of ψ for short polymer coils (*97*−*99*).

Equation A26 is the key expression we have used for analysis of our light scattering data. For each value of ξ_p/d and ϕ, eq A26 provides an analytic, albeit cumbersome, relationship between M/M_c and M_{app}/M_c. For an assumed value of ξ_p/d, in combination with an estimate or ancillary measurement of d, and the corresponding $M_c(d)$, eq A26 can be used to infer values of M that would be consistent with measured values of $M_{app}(\phi)$ in semidilute solution. We then calculate the dilute solution value $R_g°$ expected for R_g using eq A25, and similarly, the dilute solution value $R_h°$, using the Yamakawa and Fujii theory (*47*).

Having so obtained M/M_c and $R_g°/d$ consistent with the assumed ξ_p/d, we can further calculate the degree of overlap X using eq A22. Using this value of X together with experimental and theoretical results for $\xi_H/\xi_H°$ and $\xi_S/R_g°$ vs X from the literature, we can further estimate the quantities $(R_g)_{app}/R_g°$ and $(R_h)_{app}/R_h°$ that would be expected at the given degree of overlap. These then permit comparison between predicted and measured values of $(R_g)_{app}$ and $(R_h)_{app}$. Here it is important to note that, in semidilute solutions, the measured angular dependence of the intensity of the scattered light is no longer a direct measure of R_g but rather provides a measure of the static correlation range ξ_s; $(R_g)_{app} = \xi_s\sqrt{3}$.

We now outline the results of an analysis of eq A26. First, we find in the coil limit $C_L \gg \xi_p$ that $X = (\delta/3^{3/2})(M/M_c)^{1/2}(\xi_p/d)^{3/2}\phi$, and defining $X_{app} = (\delta/3^{3/2})(M_{app}/M_c)^{1/2}(\xi_p/d)^{3/2}\phi$, one obtains

$$X_{app} = X/(\Theta(X))^{1/2} \quad \text{(A27)}$$

Table 2 shows selected values of X_o, $\Theta(X_o)$, and $X_{app,o}$ and demonstrates that as $X_{app,o}$ approaches 1, the degree of overlap estimated from the measured M_{app} may be substantially less than the actual degree of overlap X_o. For example, $X_{app,o} = 1.0$ corresponds to a solution in which the actual molecular weight M is already four times as large as the apparent molecular weight, M_{app}. This suggests that caution is needed when attempting to use M_{app} to help judge whether a micellar solution that is thought to be polymerlike is in a dilute or semidilute state.

We now illustrate the results using the full form of eq A26, not in the flexible coil limit, for two choices of ξ_p/d: (1) $\xi_p/d = 4$, which corresponds to a value of ξ_p near the value 17 nm that we estimated above, and (2) $\xi_p/d = 8$, which would correspond to stiffer micelles and serves to illustrate a novel qualitative feature of the analysis. Because a full discussion of the results as a function of ξ_p/d is beyond the scope of this appendix, we have chosen two values of ξ_p close to or within the range of values that have been reported for micellar systems including the recent work of Egelhaaf and Schurtenberger (*14*) and Pederson et al. (*76*) on bile salt−PC micellar systems. For these comparisons, we also chose $\psi = \psi^*$ corresponding to a good solvent regime (*41*−*43*). We note that independent confirmation of this choice of ψ will require additional experimental and theoretical work.

For each value of M_{app}/M_c and ϕ, eq A26 yields a corresponding value of M/M_c. These values are shown in Table 3 together with the consequent $R_g°/d$ calculated by using eq A25 and $R_h°/d$ calculated by using the Yamakawa and Fujii theory (*47*) for wormlike coils as plotted in Figure 5; note that C_L/d (Figure 5) $= M/M_c$. We see from Table 3 that, under these assumptions, M/M_c would grow much more dramatically with dilution than M, since the solutions would be inferred to exhibit an increasing degree of overlap X upon dilution (see Table 3).

It remains to use the inferred values of $R_g°/d$, $R_h°/d$, and X to predict $(R_g)_{app}/d$ and $(R_h)_{app}/d$ and compare with the measured values. For this purpose, we have used the compilations of Brown and Nicolai (*92*); see also refs *35* and *36* for experimental values of $(R_g)_{app}/R_g°$ and $(R_h)_{app}/R_h° = \xi_H/R_h°$ that have been reported as functions of X. The resulting predicted values of $(R_g)_{app}/d$ and $(R_h)_{app}/d$ are shown in Table 3, together with our measured values. At the highest concentrations, the dashes for the measurement of $(R_g)_{app}/d$ indicate that the measurement had a very large standard error; these angular dependences of the scattered light were near or below the detection limit. At the low concentrations near the micellar dilution limit, the predicted and measured values of $(R_g)_{app}/d$ and $(R_h)_{app}/d$ are in very good agreement. At the higher concentrations, however, the predicted values of $(R_h)_{app}/d$ are somewhat below the measured values.

For $\xi_p/d = 8$, unlike the situation for $\xi_p/d = 4$, the relationship $M_{app}(M)$ becomes nonmonotonic in M for the plotted volume fractions $\phi = 0.02$ and higher. For ϕ corresponding to nonmonotonic $M_{app}(M)$, a given experimental value of M_{app} may clearly correspond to more than one possible value of M. Moreover, the $M_{app}(M)$ relationship becomes nearly horizontal for larger volume fractions. This indicates that there is a broad range of M which may be

consistent with a given M_{app}: indeed M_{app}/M_c in such regions is solely a function of ξ_p/d and ϕ, as expected for polymer solutions well beyond the cross over concentration. Finally, for ϕ approaching 0.1 M_{app}/M_c can easily approach values on the order of 1, as observed experimentally, even when $M/M_c > 100$. From eq A26, it can be shown that as a solution of long polymers ($M/M_c \gg 1$) is diluted, M_{app}/M_c increases and takes on specific values that are set by ξ_p/d (and ψ). This raises the possibility that our results of increasing M_{app} upon dilution may conceivably correspond to simple dilution of very long, locally cylindrical micelles. Indeed, such a possibility could provide the basis for a model exploring the close proximity of a hexagonal (H_I) phase to the isotropic micellar solution at high volume fractions (see Figure 7).

In accordance with the possibility that M/M_c is very large compared to 1 at the higher volume fractions ϕ studied, if the micelles have a sufficiently long persistence length, we have explored a set of such large, hypothetical molecular weights and proceeded to compare the values of $(R_g)_{app}$ and $(R_h)_{app}$ that would be predicted in such a case with our experimental values, using the same procedure described above for Table 3. The results of one such calculation are shown in Table 4, for the same system analyzed in Table 3 (EYPC/C = 1.2, 0.15 M NaCl).

Table 4 illustrates that reasonable values of ξ_p and d' can be found for which large micelles at high concentrations could be consistent with experimental values observed for $(R_g)_{app}$ and $(R_h)_{app}$. Table 4 shows reasonable agreement between the predicted and experimental $(R_g)_{app}/d'$ and $(R_h)_{app}/d'$ values. Here it should be noted that the present analysis does not consider the possibility that the conversion between $R_h°$ and $(R_h)_{app}$ may depend on solvent quality in a manner that is not accounted for solely through the quantity X. Also, Table 4 illustrates inferred values of X somewhat beyond those for which the theory of Ohta and Oono (*94*) may be expected to apply accurately. Nevertheless, it is possible that very large micelles may occur at the higher volume fractions assayed as well as near the dilution limit. It should also be noted that for the small M/M_c values appearing in Table 3, one has $C_L \sim \xi_p$ and therefore eq A19 should not apply without alteration. In such cases, we have verified our results with use of the straight rod second-virial approximation embodied in eq A13. An alternative approach would be to adjust the value of ψ for small C_L/ξ_p.

In summary, we have demonstrated in this appendix that disklike micelles are not likely to be compatible with our data and that reasonable agreement can be obtained between the quantities M_{app}, $(R_h)_{app}$, and $(R_g)_{app}$ predicted for wormlike coils and measured experimentally in the case of the EYPC/C = 1.2, 0.15 M NaCl micellar system. However, the same analysis shows that such micelles could be highly entangled as represented by an overlap parameter $X \gg 1$. Further, as shown by comparing Tables 3 and 4, considerable variations in micellar size and degree of overlap could yield reasonable agreement with the light scattering experiments.

APPENDIX B: THEORETICAL DEPENDENCY OF $I(\Theta)/C$ ON R_H FOR A WORMLIKE MIXED MICELLE

For monodisperse, noninteracting mixed micelles, $I(\theta)/C$ may be expressed (*7*) as

$$I(\theta)/C = \text{AMP} \tag{B1}$$

where A is a normalization constant and the scattering form factor $P = [1 + {}^1/_3 R_g{}^2 q(\theta)^2]^{-1}$ (*25*). It is convenient to choose a value of A that normalizes values of $I(\theta)/C$ to unity at an arbitrarily chosen value of $R_h = \alpha$. This is accomplished by combining eqs A9 and A11 with the expression $M = \pi r^2 \rho C_L N_a$ (Appendix A) to yield

$$A = 3\xi_p(1 + \alpha^2\beta)/(64 r^2 \alpha^2 \rho N_a) \tag{B2}$$

where $\beta = 64q(\theta)^2/27\pi$. Substituting this value of A into eq B1 yields

$$I(\theta)/C = (1/\alpha^2 + \beta) R_h{}^2/(1 + \beta R_h{}^2) \tag{B3}$$

This theoretical dependency of $I(\theta)/C$ on R_h for a wormlike mixed micelle is plotted in Figure 4 (solid line) based on the choice of Mazer et al. (*7*) of $\alpha = 5$ nm and $\theta = 90°$. For simplicity here, we have only fit the theory of Yamakawa and Fujii (*41*, *47*) to the data of Mazer et al. (*7*) in the limit $C_L \gg \xi_p$. However, we have shown elsewhere (*18*) that the full theory of Yamakawa and Fujii (*41*, *47*) can be fitted to the data of Mazer et al. (*7*), assuming $d = 5$ nm and $\xi_p = 15$ nm.

REFERENCES

1. Carey, M. C. (1988) in *Bile Acids in Health and Disease* (Northfield, T. C., Jazrawi, R. P., and Zentler-Munro, P. L., Eds.) pp 61−82, Kluwer Academic Press, Dordrecht, The Netherlands.
2. Lester, R., Carey, M. C., Little, J. M., Cooperstein, L. A., and Dowd, S. R. (1975) *Science 189*, 1098−1100.
3. Vinson, P. K., Talmon, Y., and Walter, A. (1989) *Biophys. J. 56*, 669−681.
4. Backer, J. M., and Dawidowicz, E. A. (1987) *Nature 327*, 341−343.
5. Smith, R., and Tanford, C. (1972) *J. Mol. Biol. 67*, 75−83.
6. Cabral, D. J., and Small, D. M. (1989) in *Handbook of Physiology − The Gastrointestinal System III* (Schultz, S. G., Forte, J. G., and Rauner, B. B., Eds.) pp 621−662, American Physiological Society, Bethesda, MD.
7. Mazer, N. A., Benedek, G. B., and Carey, M. C. (1980) *Biochemistry 19*, 601−615.
8. Small, D. M. (1967) *Gastroenterology 52*, 607−610.
9. Dervichian, D. G. (1968) *Adv. Chem. Ser. 84*, 78−87.
10. Hjelm, R. P., Thiyagarajan, P., and Alkan, H. (1988) *J. Appl. Crystallogr. 21*, 858−863.
11. Hjelm, R. P., Thiyagarajan, P., and Alkan-Onyuksel, H. (1992) *J. Phys. Chem. 96*, 8653−8661.
12. Nichols, J. W., and Ozarowski, J. (1990) *Biochemistry 29*, 4600−4606.
13. Walter, A., Vinson, P. K., Kaplun, A., and Talmon, Y. (1991) *Biophys. J. 60*, 1315−1325.
14. Egelhaaf, S. U., and Schurtenberger, P. (1994) *J. Phys. Chem. 98*, 8560−8573.
15. Carey, M. C., and Small, D. M. (1970) *Am. J. Med. 49*, 590−608.
16. Chamberlin, R., Thurston, G., Benedek, G., Cohen, D., and Carey, M. (1989) Materials Research Society Fall Meeting, Boston, MA, Abstract booklet, p 88, Materials Research Society, Warrendale, PA.
17. Chamberlin, R., Thurston, G., Benedek, G., Cohen, D., and Carey, M. (1989) 3rd International Symposium on Complex Fluids, Santa Barbara, CA, July 23−28.
18. Chamberlin, R. A. (1991) Ph.D. Dissertation, Massachusetts Institute of Technology, Cambridge, MA.

19. Haller, H. R., Destor, C., and Cannell, D. S. (1983) *Rev. Sci. Instrum. 54*, 973−983.
20. Cohen, D. E., Chamberlin, R. A., Thurston, G. M., Benedek, G. B., and Carey, M. C. (1991) in *Bile Acids As Therapeutic Agents* (Paumgartner, G., Stiehl, A., and Gerok, W., Eds.) pp 147−150, Kluwer Academic Press, Lancaster, U.K.
21. Cohen, D. E., and Carey, M. C. (1990) *Hepatology 12*, 143S-148S.
22. Cohen, D. E., Angelico, M., and Carey, M. C. (1990) *J. Lipid Res. 31*, 55−70.
23. Carey, M. C., and Small, D. M. (1978) *J. Clin. Invest. 61*, 998−1026.
24. Carey, M. C. (1985) in *New Comprehensive Biochemistry* (Danielsson, H., and Sjövall, J., Eds.) pp 345−403, Elsevier, Amsterdam.
25. Berne, B. J., and Pecora, R. (1976) *Dynamic Light Scattering*, John Wiley and Sons, New York.
26. Cohen, D. E., Fisch, M. R., and Carey, M. C. (1990) *Hepatology 12*, 113S-122S.
27. Earnshaw, J. C., and Steer, M. W. (1983) *The Application of Laser Light Scattering to the Study of Biological Motion*, Plenum Press, New York.
28. Koppel, D. E. (1972) *J. Chem. Phys. 57*, 4814−4820.
29. Tanford, C. (1961) *Physical Chemistry of Macromolecules*, John Wiley and Sons, New York.
30. Ollivon, M., Eidelman, O., Blumenthal, R., and Walter, A. (1988) *Biochemistry 27*, 1695−1703.
31. Donovan, J. M., Timofeyeva, N., and Carey, M. C. (1991) *J. Lipid Res. 32*, 1501−1512.
32. Small, D. M., and Bourgès, M. (1966) *Mol. Crystals 1*, 541−561.
33. Donovan, J. M., Benedek, G. B., and Carey, M. C. (1987) *Biochemistry 26*, 8116−8125.
34. Small, D. M. (1967) *J. Lipid Res. 8*, 551−557.
35. Schurtenberger, P., and Cavaco, C. (1993) *J. Phys. II France 3*, 1279−1288.
36. Schurtenberger, P., and Cavaco, C. (1994) *J. Phys. II France 4*, 305−317.
37. Schurtenberger, P., and Cavaco, C. (1996) *Langmuir 12*, 2894−2899.
38. Blankschtein, D., Thurston, G. M., and Benedek, G. B. (1986) *J. Chem. Phys. 85*, 7268−7288.
39. Kirkwood, J. G., and Goldberg, R. J. (1950) *J. Chem. Phys. 18*, 54−57.
40. Stockmayer, W. H. (1950) *J. Chem. Phys. 18*, 58−61.
41. Yamakawa, H. (1971) *Modern Theory of Polymer Solutions*, Harper and Row, New York.
42. Grosberg, A. Y., and Khokhlov, A. R. (1994) *Statistical Physics of Macromolecules*, American Institute of Physics Press, New York.
43. Freed, K. F. (1987) *Renormalization Group Theory of Macromolecules*, Wiley, New York.
44. Small, D. M., Bourgès, M., and Dervichian, D. G. (1966) *Nature 211*, 816−818.
45. Small, D. M., Bourgès, M. C., and Dervichian, D. G. (1966) *Biochim. Biophys. Acta 125*, 563−580.
46. Schurtenberger, P., Mazer, N., and Känzig, W. (1985) *J. Phys. Chem. 89*, 1042−1049.
47. Yamakawa, H., and Fujii, M. (1973) *Macromolecules 6*, 407−415.
48. Ulmius, J., Lindblöm, G., Wennerström, H., Johansson, L., Fontell, K., Soderman, O., and Arvidson, G. (1982) *Biochemistry 21*, 1553−1560.
49. Lindblöm, G., Wennerström, H., Arvidson, G., and Lindman, B. (1976) *Biophys. J. 16*, 1287−1295.
50. Fahey, D. A., Carey, M. C., and Donovan, J. M. (1995) *Biochemistry 34*, 10886−10897.
51. McCabe, R., and Carey, M. C. (1977) *Clin. Res. 25*, 468A.
52. Small, D. M. (1984) *Hepatology 4*, 180S−190S.
53. DuPré, D. B., and Yang, S. (1990) *J. Chem. Phys. 94*, 7466−7477.
54. Hentschke, R., and Herzfeld, J. (1991) *Phys. Rev. A 44*, 1148−1155.
55. Herzfeld, J. (1996) *Acc. Chem. Res. 29*, 31−37.
56. Khokhlov, A. R., and Semenov, A. N. (1982) *Physica 112A*, 605−614.
57. Crawford, J. M., Möckel, G.-M., Crawford, A. R., Hagen, S. J., Hatch, V. C., Barnes, S., Godleski, J. J., and Carey, M. C. (1995) *J. Lipid Res. 36*, 2147−2163.
58. Atkinson, D., and Small, D. M. (1986) *Annu. Rev. Biophys. Biophys. Chem. 15*, 403−456.
59. van Antwerpen, R., Chen, G.-C., Pullinger, C. R., Kane, J. P., LaBelle, M., Krauss, R. M., Luna-Chavez, C., Forte, T. M., and Gilkey, J. C. (1997) *J. Lipid Res. 38*, 659−669.
60. Perrin, F. (1936) *J. Phys. Radium 7*, 1−11.
61. Herzfeld, J., and Briehl, R. W. (1981) *Macromolecules 14*, 397−404.
62. Gelbart, W. M., Ben-Shaul, A., McMullen, W. E., and Masters, A. (1984) *J. Phys. Chem. 88*, 861−866.
63. Blankschtein, D., Thurston, G. M., and Benedek, G. B. (1985) *Phys. Rev. Lett. 54*, 955−958.
64. Goldstein, R. E. (1985) *J. Chem. Phys. 84*, 3367−3378.
65. Cates, M. E., and Candau, S. J. (1990) *J. Phys.: Condens. Matter 2*, 6869−6892.
66. van der Schoot, P., and Cates, M. E. (1994) *Langmuir 10*, 670−679.
67. Isihara, A., and Hayashida, T. (1951) *J. Phys. Soc. Jpn. 6*, 46−50.
68. Isihara, A., and Hayashida, T. (1951) *J. Phys. Soc. Jpn. 6*, 40−45.
69. Kholodenko, A. L., and Douglas, J. F. (1995) *Phys. Rev. E 51*, 1081−1090.
70. Gaigalas, A. K., Reipa, V., Hubbard, J. B., Edwards, J., and Douglas, J. (1995) *Chem. Eng. Sci. 50*, 1107−1114.
71. Boek, E. S., Coveney, P. V., Lekkerkerker, N. W., and van der Schoot, P. (1997) *Phys. Rev. E 55*, 3124−3133.
72. Kratky, O., and Porod, G. (1949) *Recl. Trav. Chim. Pays-Bas 68*, 1106−1122.
73. Schaefer, D. W., and Han, C. C. (1985) in *Dynamic Light Scattering. Applications of Photon Correlation Spectroscopy* (Pecora, R., Ed.) pp 181−243, Plenum Press, New York.
74. Long, M. A., Kaler, E. W., Lee, S. P., and Wignall, G. D. (1994) *J. Phys. Chem. 98*, 4402−4410.
75. Long, M. A., Kaler, E. W., and Lee, S. P. (1994) *Biophys. J. 67*, 1733−1742.
76. Pedersen, J. S., Egelhaaf, S., and Schurtenberger, P. (1995) *J. Phys. Chem. 99*, 1299−1305.
77. Porte, G., Appell, J., and Poggi, Y. (1980) *J. Phys. Chem. 84*, 3105−3110.
78. Hoffman, H., Rehage, H., Platz, G., Schorr, W., Thurn, H., and Ulbricht, W. (1982) *Colloid Polym. Sci. 260*, 1042−1056.
79. Candau, S. J., Hirsch, E., and Zana, R. (1984) *J. Phys. (Paris) 45*, 1263−1270.
80. Imae, T. (1988) *J. Phys. Chem. 92*, 5721−5726.
81. Mishic, J. R., and Fisch, M. R. (1990) *J. Chem. Phys. 92*, 3222−3229.
82. Jerke, G., Pedersen, J. S., Egelhaaf, S. U., and Schurtenberger, P. (1997) *Phys. Rev. E 56*, 5772−5788.
83. Lomakin, A., Chung, D. S., Benedek, G. B., Kirschner, D. A., and Teplow, D. B. (1996) *Proc. Natl. Acad. Sci. U.S.A. 93*, 1125−1129.
84. de la Torre, J. G., and Bloomfield, V. A. (1981) *Q. Rev. Biophys. 14*, 81−139.
85. Douglas, J. F., and Freed, K. F. (1984) *Macromolecules 17*, 1854−1870.
86. Wiltzius, P., Haller, H. R., Cannell, D. S., and Schaefer, D. W. (1983) *Phys. Rev. Lett. 51*, 1183−1186.
87. Ohta, T., and Oono, Y. (1982) *Phys. Lett. 89A*, 460−464.
88. Ohta, T., and Nakanishi, A. (1983) *J. Phys. A: Math. Gen.* 4155−4170.
89. Wiltzius, P., Haller, H. R., Cannell, D. S., and Schaefer, D. W. (1984) *Phys. Rev. Lett. 53*, 834−837.
90. Nakanashi, A., and Ohta, T. (1985) *J. Phys. A: Math. Gen. 18*, 127−139.

91. Shiwa, Y. (1987) *Phys. Rev. Lett. 58*, 2102−2105.
92. Brown, W., and Nicolai, T. (1990) *Colloid Polym. Sci. 268*, 977−990.
93. Cotts, P. M., and Selser, J. C. (1990) *Macromolecules 23*, 2050−2057.
94. Oono, Y. (1985) *Adv. Chem. Phys. 61*, 301−437.
95. Jinbo, Y., Sato, T., and Teramoto, A. (1994) *Macromolecules 27*, 6080−6087.
96. Doty, P., and Benoit, H. (1953) *J. Phys. Chem. 87*, 958−963.
97. Huber, K., and Stockmayer, W. H. (1987) *Macromolecules 20*, 1400−1402.
98. Yamakawa, H. (1992) *Macromolecules 25*, 1912−1916.
99. Yamakawa, H., Abe, F., and Einaga, Y. (1993) *Macromolecules 26*, 1989−1904.

BI980182Y